Research Square

Preprints are preliminary reports that have not undergone peer review.
They should not be considered conclusive, used to inform clinical practice,
or referenced by the media as validated information.

Cell polarity mediates melanoma invasion through centrosome and invadopodia positioning

Philippe Ronde

philippe.ronde@unistra.fr

UMR CNRS 7021 https://orcid.org/0000-0001-8740-1824

Yamina Boukenadel
UMR CNRS 7021

Gabrielle Boisson
UMR CNRS 7021

Rana Abdallah
UMR CNRS 7021

Marlène Legrand
UMR CNRS 7021

Hélène Justiniano
UMR CNRS 7021

Marie Zinsius
UMR CNRS 7021

Nadir Maar
UMR CNRS 7021

Grégory Adam
UMR CNRS 7021

Philippe Carl
UMR CNRS 7021

Denis Dujardin
UMR CNRS 7021 https://orcid.org/0000-0001-6372-5293

Article

Keywords: cortactin, Tks5, Pyk2, invadopodia, polarity, invasion, migration, melanoma

Posted Date: November 25th, 2026

DOI: https://doi.org/10.21203/rs.3.rs-11650670/v1

License: This work is licensed under a Creative Commons Attribution 4.0 International License.
Read Full License

Additional Declarations: (Not answered)

Cell polarity mediates melanoma invasion through centrosome and invadopodia positioning

Yamina Boukenadel[1], Gabrielle Buisson[1], Rana Abdallah[1], Marlène Legrand[1], Hélène Justiniano[1], Marie Zinsius[1], Nadir Maar[1], Grégory Adam[1], Philippe Carl[1], Denis Dujardin[1*] and Philippe Rondé[1*]

[1] Université de Strasbourg, CNRS UMR7021, Migration, Invasion et Ciblage, Faculté de Pharmacie, Illkirch, France.

*Correspondance to: Philippe Rondé, e-mail: philippe.ronde@unistra.fr, Tel. +33 3688 54184 or Denis Dujardin, e-mail: denis.dujardin@unistra.fr, Tel. +33 3688 54289

Abbreviations: ECM, extracellular matrix; MMP, matrix metalloprotease; FAK, Focal Adhesion Kinase, FA, Focal adhesion

Running title: Invadopodia positioning

Key words: cortactin, Tks5, Pyk2, invadopodia, polarity, invasion, migration, melanoma

Abstract

Cell invasion is an extremely complex process that requires polarized cell migration and directional degradation of the extracellular matrix. In melanoma cells, as in many highly invasive cancer types, these processes are governed by the controlled assembly of adhesive structures and invasive protrusions known as invadopodia. However, how migration and matrix degradation are coordinated to produce efficient cell invasion remains poorly described and a clear understanding of the mechanisms of invadopodia positioning and formation is still lacking. In this study, we examined the mechanisms of invadopodia assembly in melanoma cells using high-end imaging techniques. We show that melanoma are polarized cells thereby enabling directional migration. Our results indicate that melanoma cell polarity regulate invadopodia positioning as nascent invadopodia assemble in the vicinity of the Golgi apparatus/centrosome ahead of the nucleus and stabilized upon Tks5 arrival. Finally, we found that cytoplasmic dynein controls the localisation of the Golgi/centrosome and the formation of polarized invadopodia in melanoma cells.

Introduction

Melanoma represents one of the most aggressive human malignancies, and patients with disseminated disease exhibit a poor clinical outcome, with 5-year survival rates falling below 5%[1]. As observed in numerous invasive epithelial carcinomas—including prostate, head and neck, and breast cancers—melanoma cells acquire the capacity to traverse the basement membrane through the formation of specialized actin-dependent protrusive structures termed invadopodia. Invadopodia are subcortical, F-actin–rich membrane extensions that spatially confine proteolytic activity to sites of cell–matrix interaction and function as critical integration nodes for multiple oncogenic signaling pathways[2]. Their core is composed of a dense actin network enriched in actin nucleators, polymerization factors, and regulatory proteins, surrounded by adhesion complexes, scaffolding molecules, and signaling effectors[3]. These structures accumulate high concentrations of proteolytic enzymes, notably matrix metalloproteinases (MMPs), which mediate localized extracellular matrix (ECM) degradation and thereby facilitate invasive behavior. Substantial progress has been made in delineating the molecular mechanisms governing invadopodia biogenesis. The temporal sequence of events underlying their initiation, maturation, and functional activation is increasingly well defined, revealing a tightly coordinated interplay between cytoskeletal remodeling, adhesion dynamics, and protease trafficking[4].

Yet, one of the key questions that remains to be solved concerns the formation of invadopodia and especially the mechanism that regulates their positioning. Indeed, previous study reported that newly formed invadopodia arise from the cell periphery around lamellipodia. Moreover, invadopodium precursors were found to initiate at the proximal tip of focal adhesions[5,6]. Furthermore, in vascular smooth muscle cells, PKC activation with the tumor promoter phorbol myristate acetate has been shown to induce the formation of podosomes at sites of focal adhesion disassembly, suggesting a direct transition between the two structures[7].

In an effort to identify potential targets to limit the formation of invadopodia and reduce tumor invasiveness, Alissa Weaver's group identified PI3K and PKCα as interacting regulators of invasive behavior mediating a shift from focal adhesions to invadopodia[8]. Conversely, we recently reported that invadopodia disassembly may promote the formation of nearby focal adhesions[9]. As focal adhesion and invadopodia share many structural components and seem to be regulated by similar pathways it is thus possible that, upon specific signaling, focal adhesion disassembly generate de novo invadopodia. However, other studies indicated that invadopodia are preferentially found under or in the immediate vicinity of the nucleus suggesting that there might be some physical interaction between invadopodia and the nucleus[10]. Moreover, a recent report has shown that invasion through constricted spaces generates an adaptive response with centrosome-centered formation of invadopodia. In this case, nucleus forward-pulling forces would generate nuclear deformation triggering invadopodia assembly and matrix degradation thereby facilitating nucleus passage[11].

Cell migration is a fundamentally polarized process which involve the establishment of front–rear polarity and leading edge extension where new adhesions are formed[12]. These nascent adhesions mature into focal adhesions that enable the transmission of traction forces required for cell movement. This dynamic process involves temporal and spatial regulation of focal adhesion turn-over. Therefore, cell migration requires asymmetric dynamics of focal adhesions which is closely coupled to the reorganization of the actin cytoskeleton. The turn-over of focal adhesion is controlled by phosphorylation processes of key components such as Src, FAK or paxillin[13–15]. Microtubules play a key role in the polarized distribution of signals within a cell and thus, have been implicated in the asymmetric regulation of adhesion turn-over[16]. The ability of microtubules to differentially regulate adhesion turn-over at the leading edge and at the rear of migrating cells can be explained by the polarization of the microtubule network which involve orientation of the MTOC in the migration direction. Multiple

93 microtubule targeting of adhesions leads to their disassembly[17,18]. Microtubules-induced focal
94 adhesion turn-over is in part due to clathrin-dependent endocytosis of adhesion components and
95 activation of small GTPase-dependent pathway[19–21]. For example, activation of the
96 p130CAS/Dock180/Rac1 signaling pathway was linked to FAK phosphorylation, focal
97 adhesion turnover and lamellipodia formation[22].

98 While the polarized localization of focal adhesion is well documented much less is
99 known concerning a potential polarized distribution of invadopodia and the function of
100 microtubules in this mechanism. Nevertheless, invadopodia turn-over is also dependent upon
101 several GTPases activities, including Cdc42, RhoA, RhoC, RhoG and Rac1[23–25] which might
102 be activated by specific targeting of microtubule at invadopodia. Indeed, several plus-end
103 tracking proteins such as EB1, APC, and ACF7 have been shown to be negative regulators of
104 invadopodia formation[26]. Thus, a current research challenge is to uncover how proteolytic
105 activity is tightly controlled and localized at specific membrane sites to support targeted ECM
106 degradation at invadopodia. Especially during migration of cancer cells, how proper
107 invadopodia formation contribute to cell invasion is an important issue to elucidate.

108 In this study, we addressed the role of polarized mechanisms in melanoma migration
109 and degradation processes. Using high-end imaging techniques, we reported that melanoma
110 cells acquire increased polarity mechanism compared to melanocytes, leading to enhanced
111 directional migration. Investigating invadopodia formation processes we report that Lis1-
112 dependent centrosome orientation is implicated in nascent invadopodia positioning. Moreover,
113 in freely-moving melanoma cells we found that centrosome positioning dictate invadopodia
114 formation ahead of the nucleus in the direction of the polarity axis. Finally, we show that
115 inhibiting cell polarity using Lis1 knockdown reduced both invadopodia activity and melanoma
116 migration and invasion.

Material and methods

Antibodies

For immunofluorescence, anti-cortactin (p80/85) clone 4F11 (1/250 ; Sigma-Aldrich 05-180), anti-phospho-Y402-Pyk2 (1/250 ; Cell Signaling 3291S), anti-TKS5 (1/500 ; Invitrogen PA558169), anti-GM130 (1/500 ; BD bioscience 610823) and anti-pericentrin (1/500 ; Proteintech 60919-1) antibodies were used as primary antibodies along with Alexa Fluor 568 conjugated phalloidin (1/250 ; A12380), Alexa Fluor 488 conjugated anti-rabbit (1/1000 ; A11034), Alexa Fluor 568 conjugated anti-mouse (1/1000 ; A11004) and Alexa Fluor 647 conjugated anti-mouse (1/1000 ; A21236) antibodies were used as secondary antibodies for immunostaining assays

Cell culture

A375 melanoma cell line (ATCCR CRL-1619) was cultured in DMEM (Dulbecco's Modified Eagle Medium, GibcoTM) medium supplemented with 10% fetal bovine serum (CYTIVATM) 1% pyruvate, 1% glucose, 1% L-glutamine (BiowestTM, MS02EH) and 1% penicillin/streptomycin (respectively 100 units/mL and 50 µg/mL, Dutscher) at 37°C, 5% CO2. Primary human melanoma cell line WM983A was purchased from Rockland and cultured in Leibovitz L-15:MCDB 153 media (1:4, 11415064, Invitrogen ; M7403, Sigma) supplemented with 2% fetal bovine serum, 1.68 mM CaCl2 and 1% penicillin/streptomycin (respectively 100 units/mL and 50 µg/mL, Dutscher) at 37°C, 5% CO2. Normal human primary epidermal melanocytes (HEM), from Lonza, were cultivated inMGM-4 medium (PS-200-041, ATCC).

Cell transfection and infection

Plasmids expressing Tks5-GFP and Cortactin-dsRed were kindly provided by S. Courtneige (Oregon Health & Science University, Portland) and M.A. McNiven (Mayo Cancer Center, Rochester). Plasmids were verified by sequencing and isolated using the JetStarPlasmid kit (Genomed) according to the manufacturer's instructions. Cells were transfected with 0.5 µg of

Tks5-GFP or Cortactin-dsRed plasmids using lipofectamine 2000 (Invitrogen), or with 50 nM siRNA (ON-TARGET plus SMARTpool Human PAFAH1B1 (siLIS1) or ON-TARGET plus Non-targeting Control Pool, DharmaconTM (siCTRL)) using DharmaFECTTM according to the manufacturer's instructions. A375 melanoma cells were co-transfected with 0.5 µg Tks5-GFP plasmids and control/anti-LIS1 siRNAs (30 pmol of siRNA for each µg of DNA) using lipofectamine 2000 (Invitrogen), according to the manufacturer's instructions. Knockdown efficiency was analyzed by western blot as described below. Cells were infected with 1.7 to 2.5 µL of CellLight™ Golgi-GFP/Tubulin-RFP BacMam 2.0 (Invitrogen, C10593) reagent per 10 000 cells in media, then incubated at 37°C, 5% CO2 for 24 hours before use.

Western blotting

Cells were washed with PBS and lysed with RIPA buffer supplemented with protease and phosphatase inhibitor cocktail (HaltTM Thermo Scientific) and 1% EDTA (Thermo Scientific)) at 4°C. Cell lysates were then incubated on ice for 20 min and centrifuged at 15 700 rcf for 10 min at 4°C. Cell extracts were denatured in Laemmli buffer (4x Laemmli protein sample buffer Biorad 1610747) and 1% β-mercaptoethanol (Biorad 1610710) and incubated at 100°C for 5 min then loaded on 4-15% polyacrylamide gels (Mini-PROTEAN® TGXTM Biorad 4561086). Separated proteins were transferred to a polyvinylidene difluoride membrane (Trans-Blot Turbo Biorad 1704156) then incubated in mouse anti-GAPDH (1/5000 ; Proteintech 60004-1-IG) and mouse anti-Lis1 (1/1000 ; Biotechnology sc-17817) primary antibodies for 1 h followed by 1 h incubation in horseradish peroxidase conjugated goat anti-mouse secondary antibodies (1706516). Protein bands were detected by chemilumenescence using the Cytvia ECLTM Prime kit and images were acquired using Amersham IQ 800 GxP E-Licence.

Gelatin coating

Plasma-cleaned glass coverslips (Epredia®, 18 mm, ref. CB00180RA120MNZ0) were incubated in poly-Lysine 1X (Sigma-Aldrich, P4832-50 mL) for 20 min, then in glutaraldehyde

(Merck, ref. CS207801; G6257-10 mL) for 15 min and then in 2.5% Alexa Fluor 647 conjugated pork gelatin for 10 min with 3 PBS washes between each incubation. Gelatin-coated coverslips were kept in media at 37°C, 5% CO2 before use.

Matrix degradation assay and immunofluorescence

Melanoma cells were plated on fluorescent gelatin and incubated for indicated time in medium supplemented with 10% fetal bovine serum and 40 ng/mL EGF at 37°C, 5% CO2. Cells were fixed with 4% paraformaldehyde, permeabilized with 0.1% Triton-X-100 and incubated in 2% BSA at room temperature. Cells were then incubated in the aforementioned primary antibodies for 1 h, washed with PBS three times then incubated in secondary antibodies for 1 h at room temperature. Cells were washed in PBS, stained with Dapi (100 ng/mL, Sigma D9542) for 10 minutes, washed again and mounted in Prolong Gold mounting media (Invitrogen). Cells were imaged with Leica TCS SP8 confocal microscope (63x HCX PL APO CS2 1.40 NA objective). Invadopodia were identified as cortactin and actin rich punctiform structures. Invadopodia degradation regions were identified as black dots on fluorescent gelatin. Fluorescence intensity was quantified using ImageJ software.

CYTOO chip seeding and immunostaining

A375 melanoma cells were seeded on 700 µm² CYTOOTM chips (CW-S-FN x18 (ref. 10-004-10-18) with 6 µm fluorescent fibronectin coated micropatterns. Cells were starved in 1% FBS for 4 hours at 37°C, 5% CO2. Invadopodia formation was stimulated using complete medium supplemented with 10% FBS and 40 ng/mL EGF for 1h30 at 37°C, 5% CO2. Cells were then fixed with 4% PFA and immunostained as described before. Cells were imaged with a leica DMIRE2 microscope (100x 63x HCX PL APO 1.40 NA objective)

Wound healing assay

Melanoma cells were seeded in 12 well plates containing medium supplemented with 10% fœtal bovin serum. After 24h, confluent cell layers treated or not siLIS1 or siCTRL with were wounded with a pipet tip. Cell were then fixed with 3%PFA 4 h after wounding and

194 immunostained as described before. Images were acquired using a Leica DMIRE2 microscope
195 (x10 N PLAN 0.25 NA objective or x20 PLAN 0.40 NA).

196 ***Cell invasion and migration assay***.

197 Invasion was assessed using 24-well plates inserts (Millicell®, Merck, Ref PCEP24H48)
198 coated with 0,43 mg/ml Matrigel and migration was assessed using uncoated inserts. A375 cells
199 transfected or not were seeded on the inner part of the insert (8 µm pore size) in 200 µl DMEM
200 with 1% FBS and placed in wells containing 900 µl DMEM supplemented with 10% FBS as
201 chemoattractant. After 24 h at 37° C, cells were washed with PBS, fixed in 4%
202 paraformaldehyde and stained with 40,6-diamidino- 2-phenylindole (DAPI). Invading and
203 migrating cells were counted using an epifluorescence microscope.

204 ***Live cell imaging, and FRAP experiments***

205 For live cell imaging, cells were plated on fluorescent gelatin-coated coverslips and mounted
206 in a Ludin Chamber (Life Imaging Services) then observed at 37°C, 5% CO2 on an iMIC
207 microscope with a multi-LED Lumencor SpectraX, an Olympus 60x TIRFM 1.45 NA objective
208 and a Hamamatsu Flash 4 V2+ camera (Iwata). Images were acquired using the Live
209 Acquisition (Till Photonic) software every 2.5 minutes for a total period of 5 hours. Around 30
210 fields were acquired for each experiment. FRAP experiments were done at 37°C, 5% CO_2 on a
211 iMIC microscope. Briefly, fluorescence intensity was measured at low laser power before
212 bleach in selected regions of interest at invadopodia. Photobleaching was done at 100% of the
213 491 or 565 nm line with 4 iterations. Recovery was followed at various time intervals until the
214 intensity had reached a steady plateau. For each time point, the intensity of the bleached area
215 was normalized to that of a corresponding unbleached area. Fluorescence during recovery was
216 normalized to the prebleached intensity. FRAP measurements were fitted to a single
217 exponential curve, $I(t) = I(0) + k1e^{-k2t}$ to determine the characteristic time of recovery.

218

Statistical analysis

Statistical analysis and graphical representations were conducted using Prism® (GraphPad Software 5.04). Statistical significance was calculated using Student's *t* test or One-way analysis of variance (ANOVA) test followed by Tukey's or Dunn's multiple comparison test. Significance level was set to 5% (α=0.05). For all figures, p-values were represented using one or multiple stars according to the following: *P < 0.05 ; **P < 0.01 ; ***P < 0.001 ; ****P < 0.0001.

Results

Cortactin is a marker of nascent invadopodia

To elucidate the specific role of invadopodia related-protein during invadopodia formation, we first analysed the recruitment of selective proteins at these sites using immunofluorescent experiments. For this purpose, melanoma cells were plated on gelatin-coated coverslips and invadopodia were stimulated using EGF. We found that, after 1h adhesion, many invadopodia were identified using dot-like actin/cortacin colocalisation but none of them were able to degrade the fluorescent gelatin (Figure 1A and B, top, see quantification of the gelatin signal in black along the white lines). At this time-point, cortactin and actin labelled well defined cortical structures whereas Tks5 labelling was more diffuse and P-Pyk2 only present at focal adhesions. It should be noted that Tks5 co-localized with actin and cortactin at dot-like structures in 20 to 30% of the cells analyzed suggesting latter arrival of Tks5 at invadopodia precursor (Figure 1A, top). In close opposition, at later time-point colocalisation of actin, cortactin, Tks5 and P-Pyk2 revealed active invadopodia characterized by their degradative properties as reported by *in-situ* zymography assay (Figure 1A and B, bottom). Of note, quantification of cortactin and actin signal at invadopodia revealed that the ratio of cortactin over actin decrease over time indicating further polymerisation of actin (Figure 1C). Moreover, the presence of both markers at early time point before the acquisition of degradative capacity indicate that actin and cortactin are marker of invadopodia precursors. To confirm the identity of these actin- and cortactin-rich structures we next used time-lapse videomicroscopy. We first verified the correct localisation of Cortactin-dsRed and Tks5-GFP by immunocytochemistry (Supplemental Figure 1). In A375 cells transfected with Cortactin-dsRed and Tks5-GFP and plated on fluorescent gelatin, we found that cortactin assemble at dot-like structures that are highly dynamic (arrowheads, Figure 2A, Video 1). Quantification of cortactin fluorescence indicate cortactin fluctuations at several discrete sites which may correspond to the previously described invadopodia precursors (Figure

2B, top). Many of these precursors did not mature into degradative invadopodia as indicated by the lack of gelatin degradation sites during the time-course of the experiment (Figure 2A). However, some of these precursors displayed a maturation process leading to active invadopodia. We found that this maturation step take place upon Tks5 arrival at invadopodia precursor (arrow, Figure 2A). It is interesting to note that at this sites, cortactin and Tks5 fluctuations are synchronised until gelatin degradation (see invadopodia 2 and 3, Figure 2B, bottom). To further evaluate whether cortactin and Tks5 displayed similar dynamics at invadopodia we performed FRAP experiments. Using these technics, we reported that cortactin displayed very fast kinetic at invadopodia precursors ($t_{1/2}$ = 2.61 ± 0.61 s) which significantly increase upon Tks5 arrival ($t_{1/2}$ = 4.69 ± 1.03 s) being comparable to Tks5 recovery time ($t_{1/2}$ = 5.20 ± 0.71 s) (Figure 2C). As Tks5 has been shown to interact with cortactin[27], these results strongly suggest that cortactin is involved in invadopodia precursor assembly that mature into degradative invadopodia upon cortactin/Tks5 interaction.

Invadopodia assemble near the centrosome

In our previous immunofluorescence experiments, we noticed that invadopodia were formed near the nucleus at early time-point. Recently, invadopodia were found to localize in front of the centrosome in invasive breast cancer cells migrating into a high density collagen layer[11]. We thus sought to determine the role of the centrosome and associated microtubule organizing centres such as the Golgi in positioning invadopodia in invasive melanoma cells. Immunofluorescent labelling of endogenous Tks5 and the Golgi marker GM130 in A375 cells showed accumulation of Tks5 spots near the Golgi at early adhesion time whereas at later adhesion time Tks5 was often located under the nucleus (Figure 3A). We thus calculate the centroid of Tks5 and Golgi labelled structures to evaluate the relative distance between Tks5-containing invadopodia and the Golgi. As indicated in Figure 3A, these distances increased over time ranging from 0,64 µm at 1h to 5,67 µm after 2h30min adhesion. Similar results were

obtained using the centrosomal marker pericentrin (Figure 3B) suggesting that invadopodia formation take place at the proximity to the Goli/centrosome. To analyse in further details the relationship between invadopodia formation and the Golgi/centrosome, we performed live-imaging of melanoma A375 cells expressing both Tks5-GFP and the human Golgi resident enzyme N-acetylgalactosaminyltransferase-RFP. As reported previously, we observed that Tks5 arrival at invadopodia take place several minutes before invadopodia displayed degradative properties (Figure 4A, Video 2). At this time, invadopodia is positioned in close proximity to the Golgi as quantified by the plot profile of Tks5 and Golgi fluorescence (Figure 4B, top). However, 10 min latter, as the cell migrated forward, invadopodia was no longer in proximity to the Golgi confirming the results obtained by immunofluorescence. Altogether these results suggest that invadopodia precusors assemble in the vicinity of the Golgi/centrosome.

Melanoma are polarized cells

Centrosome positioning during cell migration is a hallmark of cell polarity induced by the cell response to microenvironment cues. During the time-course of the time-lapse experiments we often observed Golgi positioning in front of the nucleus suggesting a polarity mechanism. To test whether melanoma are polarized cells able to response to the microenvironment by adapting the organization of their cytoskeleton we used the well accepted wound healing assay in which cells move toward the wound. In this model, polarized cells are able to orient their centrosome in front of the nucleus toward the migration axis. The latter was defined here by a line starting from the centroid of the nucleus and perpendicular to the wound direction whereas the polarity axis was defined by a line starting from the centroid of the nucleus and passing through the centroid of the Golgi apparatus. To evaluate the proportion of cells able to polarize, we analyzed the centrosome localization related to the migration axis and used a polarity angle limit of 45° as a cut off value to estimate whether the cells are polarized or not (Figure 5A, left).

We compared normal human melanocyte (HEM) with two in-situ human melanoma cells WM983A and A375 and found that 70 to 72% of melanoma cells are able to polarized whereas only 42% of melanocyte displayed such ability. Indeed, melanoma cells displayed lower polarity angle, 41,19° ± 1,96 and 35,44° ± 1,36 for WM983A and A375 cells respectively as compared to HEM cells (73,18° ± 1,89), indicating enhanced abilities for Golgi positioning in the direction of migration (Figure 5A, right). Re-orientation of the centrosome in the direction of migration is an active mechanism aimed at maintaining migration directionality. Thus, we combined live cell imaging with the wound-healing model to analyze directionality define as the effective distance over the total migration distance (Figure 5B, left). The results clearly show that melanoma cells displayed higher directionality index as compared to normal melanocyte. Moreover, using live cell imaging of A375 cells expressing tubulin-RFP we show that, in freely moving melanoma cells, the centrosome is located ahead of the nucleus in the direction of migration (Figure 5C, Video 3). Of note, in cells expressing both tubulin-RFP and Tks5-GFP we frequently observed Tks5 localization at microtubules, as previously reported in fixed cells using methanol conditions[28], together with dot-like accumulation of Tks5 travelling along these structures during the time-course of the experiment (Figure 5D). Besides, in rapidly moving cells, Tks5 did not assemble into immobilized dot-like structures precursor of mature invadopodia but appear concentrated at microtubules and the centrosome (Figure 5E, Video 4). In these cells no degradation could be observed confirming our previous study indicating that migration and matrix degradation are mutually exclusive[9]. Taken together, these observations demonstrate that melanoma cells acquire polarity mechanisms required for enhanced migration processes.

Centrosome localization regulate invadopodia precursor positioning

To further evaluate the involvement of the centrosome in positioning invadopodia precusors, A375 melanoma cells were cultured on micro-patterns. Indeed, micropatterning

allows for study of cells with reproducible shapes and facilitates the comparison and quantitative positional analysis of centrosome and nascent invadopodia. For this purpose, A375 cells were seeded on the so-called crossbow patterns, which enable the reproduction of an elongated and polarized morphology, and left to adhere for 4 hours in a medium deficient in SVF, which blocks the formation of invadopodia. Their formation was then stimulated for 1 hour 30 minutes by adding 10% SVF and 40 ng/ml EGF. The location of the Golgi/Centrosome was determined by detecting the GM130 protein. In order to position the Golgi/Centrosome relative to the nucleus, the precise location of these structures was determined using the centroid of the Golgi signal and the centroid of the nuclear area. The position of the centroid of the Golgi of each cell was then catalogued according to its proportion on four 90° quadrants centred on the nucleus of each cell, with the pink quadrant pointing towards the front of the cell (Figure 6A). The results show that the majority of the Golgi was positioned at the front of the nucleus confirming our previous experiments describing polarized mechanisms in melanoma cells. Next, we tested whether the dynein-dependant mechanism implicated in centrosome orientation during fibroblast migration was efficient in melanoma cells. For this, the Lis1 protein, encoded by the PAFAH1B1 gene, was selected as a target because it is an essential regulator of dynein, interacting directly with its motor domain and its ability to generate force[29]. We first shown by Western blot that the inhibition of Lis1 synthesis by siRNA induced a significant decrease of Lis1 protein expression in A 375 cells (Figure 6A, top right). Subsequently, we observed that the percentage of Golgi positioned at the front of the nucleus decreased significantly in cells treated with siLis1 (29.8%) as compared to cells treated with siCTRL (57.3%) and untransfected cells (48.5%, Figures 6A and B). These results indicated that the cytoplasmic dynein is necessary for the positioning of the Golgi/centrosome at the front of the nucleus in A375 melanoma cells. We next tested whether the position of the Golgi/centrosome affected the localisation of invadopodia precursors. Invadopodia precursors were determined using co-

localisation of actin and cortactin. Of note as reported previously, we found increased cortactin staining as compared to actin in these precursors. Using these markers, we observed a 28% decrease of invadopodia precursors located in the quadrant facing the front of the cell when Lis1 synthesis was inhibited (Figure 6B). Moreover, upon Lis1 inhibition we also detected an increase in Inter-Organelle Distance (IOD), which represents the average of distances between all invadopodia precursors. Altogether, these results clearly indicate that the position of the Golgi/centrosome regulate the localisation of invadopodia precursors in A375 melanoma cells.

Lis1 control polarized invadopodia formation in freely moving melanoma cells

To examine the role of the Golgi/centrosome in regulating invadopodia formation in freely moving cells, we performed live-imaging of melanoma cells expressing both Tks5-GFP and the human Golgi resident enzyme N-acetylgalactosaminyltransferase-RFP and plated on fluorescent gelatin-coated coverslips. In these cells, the nuclei were detected using the bright filed images and, at each time point, the centroid of the Golgi (green circle, Figure 7A, right) and the centroid of the nucleus (blue circle, Figure 7A, right) were calculated in order to define the polarity axis (red arrow, Figure 7A, right). During the time course of the experiments, each invadopodia position was determined (cyan circle, Figure 7A, right) and categorized into one of the four 90° quadrants (white line) centred on the nucleus of each cell. The Q1 quadrant was defined as being centred on the polarity axis (Figure 7A, right) whereas Q2, Q3 and Q4 are the following clockwise quadrants respectively. Of note, invadopodia positions were defined at the time of the first appearance of stable Tks5 signal which often take place several minute before invadopodia acquire degradative capabilities (arrows, Figure 7A). Using this analysis pipeline, we noticed that the number of invadopodia being formed in the Q1 quadrant is significantly higher from the number of invadopodia formed in the other quadrants in untreated cells (Figure 7A, bottom right) and in siControl-treated cells (Figure 7B, bottom right, Video 5) suggesting that melanoma polarity is involved in invadopodia positioning. As we previously reported that

Lis1 inhibition altered the polarised distribution of invadopodia precursor on cells cultured on micro-patterns, we thus analysed the role of Lis1 on invadopodia localisation in freely moving cells. We observed that invadopodia formation are distributed randomly in each of the four quadrants in Lis1-depleted cells (Figure 7C, Video 6). These results indicate that cell polarity control invadopodia positioning in melanoma cells.

Lis1 knock-down reduce melanoma cell migration and invasion

To examine the ability of Lis1 to regulate MMP-mediated ECM degradation by mature invadopodia, control and Lis1-knockdown cells were plated on fluorescent gelatin and allowed to degrade (Figure 8A). Quantification of the degradation area revealed a significant decrease in the ability of Lis1-depleted cells to degrade the ECM. However, as Lis1 regulates polarized formation of invadopodia, we hypothesized that it might also regulate the ability of cells to invade through an ECM barrier. To test this hypothesis, we examined the capacity of serum-starved control, and Lis1-knockdown cells to invade through Matrigel-coated membranes toward complete medium. As demonstrated in Figure 8B, Lis1-knockdown cells exhibited a reduction in proteolysis-dependent invasion through Matrigel-coated membranes. To investigate whether the decreased ability of Lis-knockdown cells to invade may also results from other mechanisms such as reduced migration, we performed the transwell migration assay using uncoated membranes. As shown in Figure 8B, Lis-knockdown cells exhibited also reduce migration through uncoated membranes toward complete medium. To further examine the ability of Lis1-depleted cells to migrate in 2D, live cell imaging was performed and control or knockdown cells were allowed to migrate in the wound-healing model. We observed that Lis1-depleted cells showed both reduced migration speed and directionality as demonstrated in Figure 8C. These results clearly indicate that, by inhibiting centrosome and invadopodia positioning, Lis1 altered melanoma cell migration parameters such as speed and directionality and invadopodia activity thereby inhibiting melanoma invasion.

Discussion

Using micropatterning, live-cell video microscopy and FRAP analysis, we have characterized the mechanism of invadopodia positioning in melanoma cells adhering to a thin 2D matrix. To our knowledge, this is the first demonstration that melanoma cells acquire polarity mechanisms implicated in both enhanced migration directionality and invadopodia formation leading to increased invasion capabilities.

In this study, we observed nascent invadopodia formation composed of invadopodia precursors enriched in F-actin and cortactin that stabilized upon Tks5 interaction and mature after Pyk2 activation. Tracking and quantification of invadopodia precusors indicate short-lasting actin-cortactin complexes that upon Tks5 recruitment possibly via cortactin[27] or alternatively N-WAST interaction[30] stabilized at specific sub-cellular domains to promote further actin polymerisation, as revealed by the change in actin/cortactin ratio over time, and ultimately invadopodia elongation. Interestingly, the synchronized oscillations of the cortactin and Tks5 signals observed upon Tks5 recruitment to invadopodia precursors indicate the formation of a stable complex as shown by the similar time diffusion observed in the FRAP experiments. These oscillations of protein complexes most certainly reflect cycles of invadopodia protrusions and retractions as reported previously in breast carcinoma[31]. As these oscillations take place several minutes before MMP-mediate gelatin degradation, it is possible that they may contribute to MMP delivery at invadopodia in agreement with previous studies indicating that rapid invadopodia protrusion-retraction cycles synchronized with calcium spikes lead to more frequent MT1-MMP delivery[31]. Indeed, recent studies indicate that Tks5 integrates vesicular trafficking pathways, such as Rab GTPase-dependent transport, with localized proteolysis, thereby coupling invadopodia dynamics to extracellular matrix degradation[32]. Moreover, endosomal trafficking of Tks5 has already been observed in breast cancer cells[33]

428 which is in line with our observation showing localisation of Tks5 at microtubules and at hot
429 spots travelling along microtubules.

430 We observed formation of invadopodia precursor near the centrosome/Golgi at early time
431 point of the adhesion and migration processes in both fixed cells, upon micropatterning and on
432 living cells. Closer observations revealed that invadopodia appear as fixed structures relative to
433 the ECM (Figure 4, Video 2) and thus, upon melanoma migration, the relative distance between
434 invadopodia and other subcellular structures such as the centrosome/Golgi were modified. This
435 is surprising in view of both the rapid turn-over of invadopodia proteins and the invadopodia
436 elongation/retraction cycles and suggest that signalling and/or adhesion protein define stable
437 invadopodia positioning. The positioning of organelles and sub-cellular structures often rely on
438 polarity mechanism and may vary during tumoral progression as we reported recently[34]. Here
439 we show that melanoma cells exhibited increased polarity properties as compared to
440 melanocytes. This led to enhanced migration directionality and to invadopodia formation along
441 the polarity axis. In both cases the mechanism implicated Lis1-dependant orientation of the
442 centrosome/Golgi toward the leading edge suggesting a cross-talk between migration and
443 invasion pathways. Lis1 has an essential role in the formation of dynein–dynactin–adaptor
444 complex and dynein has been shown to regulate centrosome orientation on fibroblast via FAK
445 interaction[35]. Moreover, dynein intermediate chain 2 interact and locate inositol
446 hexakisphosphate kinases to the leading edge where they promote focal adhesion turn-over [36].
447 Recently in breast cancer cells, Lis1 was also implicated in MT1-MMP endosome polarization
448 leading to enhanced pericellular proteolysis of confining collagen fibrils[11]. Taken together with
449 our data, these set of experiments indicate that the Lis1/Dynein complex is essential to provide
450 polarity signals controlling migration and invasion pathways. Indeed, we observed a clear
451 inhibition of melanoma migration and invasion upon Lis1 knockdown which involve both a
452 decrease in ECM degradation and a reduction of the migration speed and directionality.

One of the central actors of cell polarity is Cdc42 which control the localization of lamellipodial activity at the cell front and the reorientation of the Golgi in the direction of movement[37]. Indeed, the Cdc42 guanine exchange factor βPIX interact with Scrib to control the orientation of the microtubules network and the position of the centrosome/Golgi relative to that of the nucleus[38]. βPIX can also be phosphorylated by FAK thereby facilitated the targeting of activated Rac to focal adhesions and the turn-over of these structures[39]. Moreover, another guanine nucleotide exchange factor for Cdc42, FDG1 has been shown to interact with Tks5 and mediate polarized distribution of MT1-MMP-containing vesicles[40]. The relationship between Cdc42 pathway and the Lis1/Dynein complex-mediated organelle polarity studied here has already been established. Indeed, previous studies have shown that Nudel, a cytoplasmic dynein regulator, competes with Cdc42 for binding Cdc42GAP and consequently, mediated activation of Cdc42 thus promoting migration[41]. Moreover, during wound-induced cell migration, Cdc42 acts through the polarity protein Dlg1 to regulate the interaction of dynein with microtubules at the cell front thereby regulating centrosome positioning[42]. Finally, during neuronal motility Lis1 promotes Cdc42 activation through interaction with the GTPase IQGAP1, thus allowing membrane localization of IQGAP1 and CLIP170 thereby tethering microtubule ends to the cortical actin cytoskeleton[43].

Altogether our work highlights a new polarity mechanism that control centrosome/Golgi-mediated migration and invadopodia positioning thus allowing enhanced melanoma invasion capabilities. As melanoma invasion was reduced upon Lis1 knockdown, the characterisation of the molecular complex involved in this polarity network will be of crucial importance to test whether this complex could be druggable.

Author Contributions: Y.B., G.B., R.A, M.L. and P.C. contributed to the study design, performed data acquisition, analysis and interpretation. H.J., M.Z., N.M. performed data

acquisition and analysis. P.C. developed ImageJ macro. G.A. helped with data analysis and interpretation. P.R. and D.D. conceived, designed and supervised the research. P.R. and Y.B. wrote the manuscript. All authors critically read and approved the final manuscript.

***Funding**:* This work was in part supported by the CNRS, the Université de Strasbourg, La Ligue Contre le Cancer, Alsace contre le Cancer, the NANOTUMOR / Plan Cancer and the ITMO Cancer (ColorME, 22P096-00). GA and ML were recipient of a Fellowship from the Ministère de la Recherche. YB was recipient of a Fellowship from La Ligue Contre le Cancer.

Conflict of interest. The authors declare that they have no conflict of interest.

Bibliography

1 Shain AH, Bastian BC. From melanocytes to melanomas. *Nat Rev Cancer* 2016; **16**: 345–358.

2 Hoshino D, Branch KM, Weaver AM. Signaling inputs to invadopodia and podosomes. *J Cell Sci* 2013; **126**: 2979–2989.

3 Murphy DA, Courtneidge SA. The 'ins' and 'outs' of podosomes and invadopodia: characteristics, formation and function. *Nat Rev Mol Cell Biol* 2011; **12**: 413–426.

4 Eddy RJ, Weidmann MD, Sharma VP, Condeelis JS. Tumor Cell Invadopodia: Invasive Protrusions that Orchestrate Metastasis. *Trends Cell Biol* 2017; **27**: 595–607.

5 Yamaguchi H, Lorenz M, Kempiak S, Sarmiento C, Coniglio S, Symons M *et al.* Molecular mechanisms of invadopodium formation: the role of the N-WASP-Arp2/3 complex pathway and cofilin. *J Cell Biol* 2005; **168**: 441–452.

6 Sharma VP, Eddy R, Entenberg D, Kai M, Gertler FB, Condeelis J. Tks5 and SHIP2 regulate invadopodium maturation, but not initiation, in breast carcinoma cells. *Curr Biol* 2013; **23**: 2079–2089.

7 Kaverina I, Stradal TEB, Gimona M. Podosome formation in cultured A7r5 vascular smooth muscle cells requires Arp2/3-dependent de-novo actin polymerization at discrete microdomains. *J Cell Sci* 2003; **116**: 4915–4924.

8 Hoshino D, Jourquin J, Emmons SW, Miller T, Goldgof M, Costello K *et al.* Network analysis of the focal adhesion to invadopodia transition identifies a PI3K-PKCα invasive signaling axis. *Sci Signal* 2012; **5**: ra66.

9 Legrand M, Mousson A, Carl P, Rossé L, Justiniano H, Gies J-P *et al.* Protein dynamics at invadopodia control invasion-migration transitions in melanoma cells. *Cell Death Dis* 2023; **14**: 190.

10 Revach O-Y, Weiner A, Rechav K, Sabanay I, Livne A, Geiger B. Mechanical interplay between invadopodia and the nucleus in cultured cancer cells. *Sci Rep* 2015; **5**: 9466.

11 Infante E, Castagnino A, Ferrari R, Monteiro P, Agüera-González S, Paul-Gilloteaux P *et al.* LINC complex-Lis1 interplay controls MT1-MMP matrix digest-on-demand response for confined tumor cell migration. *Nat Commun* 2018; **9**: 2443.

12 Seetharaman S, Etienne-Manneville S. Cytoskeletal Crosstalk in Cell Migration. *Trends Cell Biol* 2020; **30**: 720–735.

13 Webb DJ, Donais K, Whitmore LA, Thomas SM, Turner CE, Parsons JT *et al.* FAK-Src signalling through paxillin, ERK and MLCK regulates adhesion disassembly. *Nat Cell Biol* 2004; **6**: 154–161.

14 Hamadi A, Bouali M, Dontenwill M, Stoeckel H, Takeda K, Rondé P. Regulation of focal adhesion dynamics and disassembly by phosphorylation of FAK at tyrosine 397. *J Cell Sci* 2005; **118**: 4415–4425.

15 Zaidel-Bar R, Milo R, Kam Z, Geiger B. A paxillin tyrosine phosphorylation switch regulates the assembly and form of cell-matrix adhesions. *J Cell Sci* 2007; **120**: 137–148.

16 Broussard JA, Webb DJ, Kaverina I. Asymmetric focal adhesion disassembly in motile cells. *Curr Opin Cell Biol* 2008; **20**: 85–90.

17 Kaverina I, Krylyshkina O, Small JV. Microtubule targeting of substrate contacts promotes their relaxation and dissociation. *J Cell Biol* 1999; **146**: 1033–1044.

18 Krylyshkina O, Anderson KI, Kaverina I, Upmann I, Manstein DJ, Small JV *et al.* Nanometer targeting of microtubules to focal adhesions. *J Cell Biol* 2003; **161**: 853–859.

19 Ezratty EJ, Bertaux C, Marcantonio EE, Gundersen GG. Clathrin mediates integrin endocytosis for focal adhesion disassembly in migrating cells. *J Cell Biol* 2009; **187**: 733–747.

20 Rooney C, White G, Nazgiewicz A, Woodcock SA, Anderson KI, Ballestrem C *et al.* The Rac activator STEF (Tiam2) regulates cell migration by microtubule-mediated focal adhesion disassembly. *EMBO Rep* 2010; **11**: 292–298.

21 Nayal A, Webb DJ, Brown CM, Schaefer EM, Vicente-Manzanares M, Horwitz AR. Paxillin phosphorylation at Ser273 localizes a GIT1-PIX-PAK complex and regulates adhesion and protrusion dynamics. *J Cell Biol* 2006; **173**: 587–589.

22 Deramaudt TB, Dujardin D, Hamadi A, Noulet F, Kolli K, De Mey J *et al.* FAK phosphorylation at Tyr-925 regulates cross-talk between focal adhesion turnover and cell protrusion. *Mol Biol Cell* 2011; **22**: 964–975.

23 Ayala I, Giacchetti G, Caldieri G, Attanasio F, Mariggiò S, Tetè S *et al.* Faciogenital dysplasia protein Fgd1 regulates invadopodia biogenesis and extracellular matrix degradation and is up-regulated in prostate and breast cancer. *Cancer Res* 2009; **69**: 747–752.

24 Goicoechea SM, Zinn A, Awadia SS, Snyder K, Garcia-Mata R. A RhoG-mediated signaling pathway that modulates invadopodia dynamics in breast cancer cells. *J Cell Sci* 2017; **130**: 1064–1077.

25 Spuul P, Ciufici P, Veillat V, Leclercq A, Daubon T, Kramer IJ *et al.* Importance of RhoGTPases in formation, characteristics, and functions of invadosomes. *Small GTPases* 2014; **5**: e28195.

26 Chanez B, Ostacolo K, Badache A, Thuault S. EB1 Restricts Breast Cancer Cell Invadopodia Formation and Matrix Proteolysis via FAK. *Cells* 2021; **10**: 388.

27 Thuault S, Mamelonet C, Salameh J, Ostacolo K, Chanez B, Salaün D *et al.* A proximity-labeling proteomic approach to investigate invadopodia molecular landscape in breast cancer cells. *Sci Rep* 2020; **10**: 6787.

28 Inoue H, Kanda T, Hayashi G, Munenaga R, Yoshida M, Hasegawa K *et al.* A MAP1B-cortactin-Tks5 axis regulates TNBC invasion and tumorigenesis. *J Cell Biol* 2024; **223**: e202303102.

29 Vallee RB, Tsai J-W. The cellular roles of the lissencephaly gene LIS1, and what they tell us about brain development. *Genes Dev* 2006; **20**: 1384–1393.

30 Oikawa T, Itoh T, Takenawa T. Sequential signals toward podosome formation in NIH-src cells. *J Cell Biol* 2008; **182**: 157–169.

31 Pourfarhangi KE, Bergman A, Gligorijevic B. ECM Cross-Linking Regulates Invadopodia Dynamics. *Biophys J* 2018; **114**: 1455–1466.

32 Jacob A, Jing J, Lee J, Schedin P, Gilbert SM, Peden AA *et al.* Rab40b regulates trafficking of MMP2 and MMP9 during invadopodia formation and invasion of breast cancer cells. *J Cell Sci* 2013; **126**: 4647–4658.

33 Iizuka S, Quintavalle M, Navarro JC, Gribbin KP, Ardecky RJ, Abelman MM *et al.* Serine-Threonine Kinase TAO3-Mediated Trafficking of Endosomes Containing the Invadopodia Scaffold TKS5α Promotes Cancer Invasion and Tumor Growth. *Cancer Res* 2021; **81**: 1472–1485.

34 Jerabkova-Roda K, Peralta M, Huang K-J, Mousson A, Bourgeat Maudru C, Bochler L *et al.* Peripheral positioning of lysosomes supports melanoma aggressiveness. *Nat Commun* 2025; **16**: 3375.

35 Fructuoso M, Legrand M, Mousson A, Steffan T, Vauchelles R, De Mey J *et al.* FAK regulates dynein localisation and cell polarity in migrating mouse fibroblasts. *Biol Cell* 2020; **112**: 53–72.

36 Rojas T, Cheng W, Gao Z, Liu X, Wang Y, Malla AP *et al.* Inositol hexakisphosphate kinase 3 promotes focal adhesion turnover via interactions with dynein intermediate chain 2. *Proc Natl Acad Sci U S A* 2019; **116**: 3278–3287.

37 Nobes CD, Hall A. Rho GTPases control polarity, protrusion, and adhesion during cell movement. *J Cell Biol* 1999; **144**: 1235–1244.

38 Osmani N, Vitale N, Borg J-P, Etienne-Manneville S. Scrib controls Cdc42 localization and activity to promote cell polarization during astrocyte migration. *Curr Biol* 2006; **16**: 2395–2405.

39 Chang F, Lemmon CA, Park D, Romer LH. FAK potentiates Rac1 activation and localization to matrix adhesion sites: a role for betaPIX. *Mol Biol Cell* 2007; **18**: 253–264.

40 Zagryazhskaya-Masson A, Monteiro P, Macé A-S, Castagnino A, Ferrari R, Infante E *et al.* Intersection of TKS5 and FGD1/CDC42 signaling cascades directs the formation of invadopodia. *J Cell Biol* 2020; **219**: e201910132.

41 Shen Y, Li N, Wu S, Zhou Y, Shan Y, Zhang Q *et al.* Nudel binds Cdc42GAP to modulate Cdc42 activity at the leading edge of migrating cells. *Dev Cell* 2008; **14**: 342–353.

42 Manneville J-B, Jehanno M, Etienne-Manneville S. Dlg1 binds GKAP to control dynein association with microtubules, centrosome positioning, and cell polarity. *J Cell Biol* 2010; **191**: 585–598.

43 Kholmanskikh SS, Koeller HB, Wynshaw-Boris A, Gomez T, Letourneau PC, Ross ME. Calcium-dependent interaction of Lis1 with IQGAP1 and Cdc42 promotes neuronal motility. *Nat Neurosci* 2006; **9**: 50–57.

596 **Figure Legends**

597

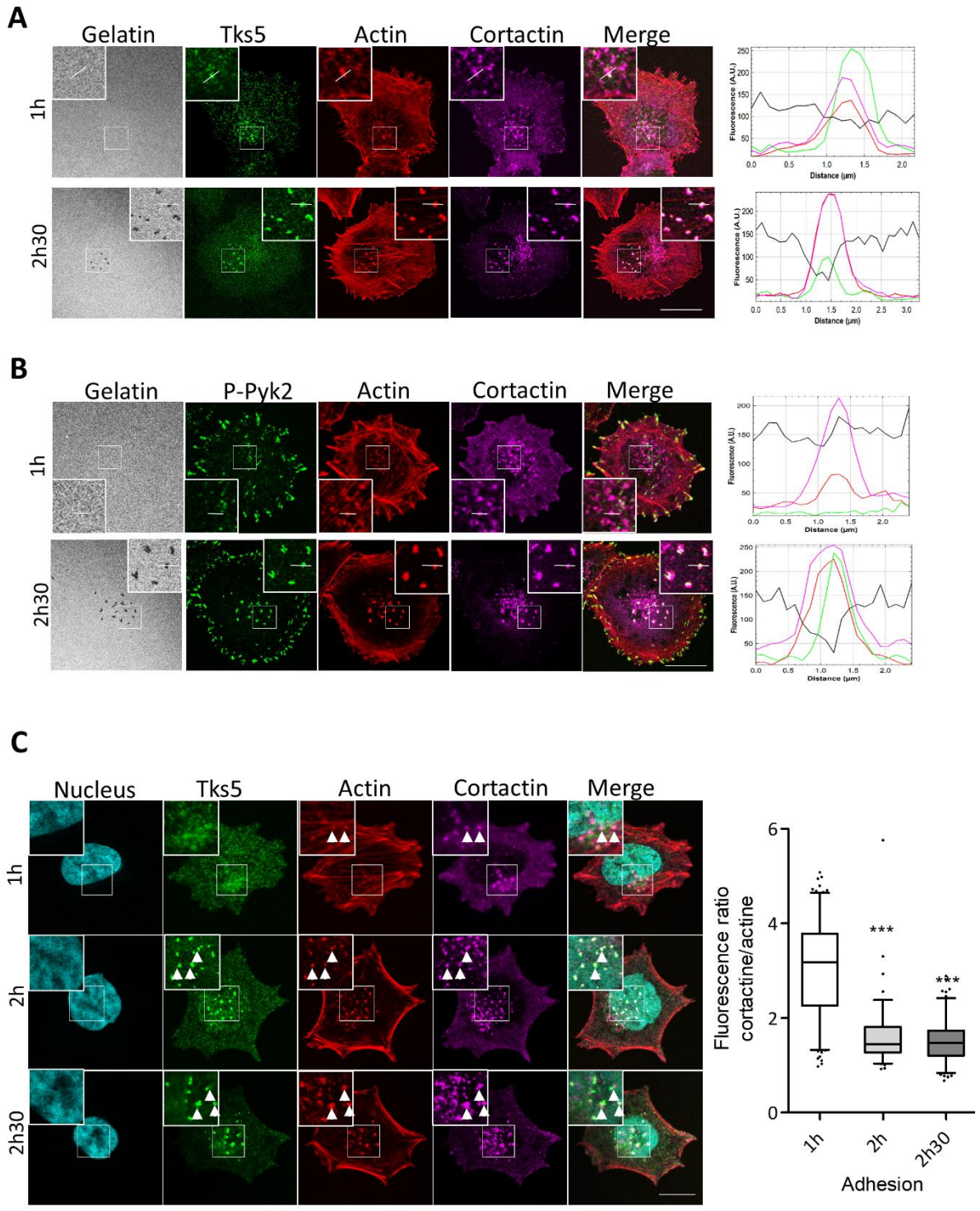
A
Gelatin
Tks5
Actin
Cortactin
Merge
1h
2h30
Fluorescence (A.U.)
Distance (µm)
B
Gelatin
P-Pyk2
Actin
Cortactin
Merge
1h
2h30
Fluorescence (A.U.)
Distance (µm)
C
Nucleus
Tks5
Actin
Cortactin
Merge
1h
2h
2h30
Fluorescence ratio cortactine/actine
***
***
1h
2h
2h30
Adhesion

Figure 1

598

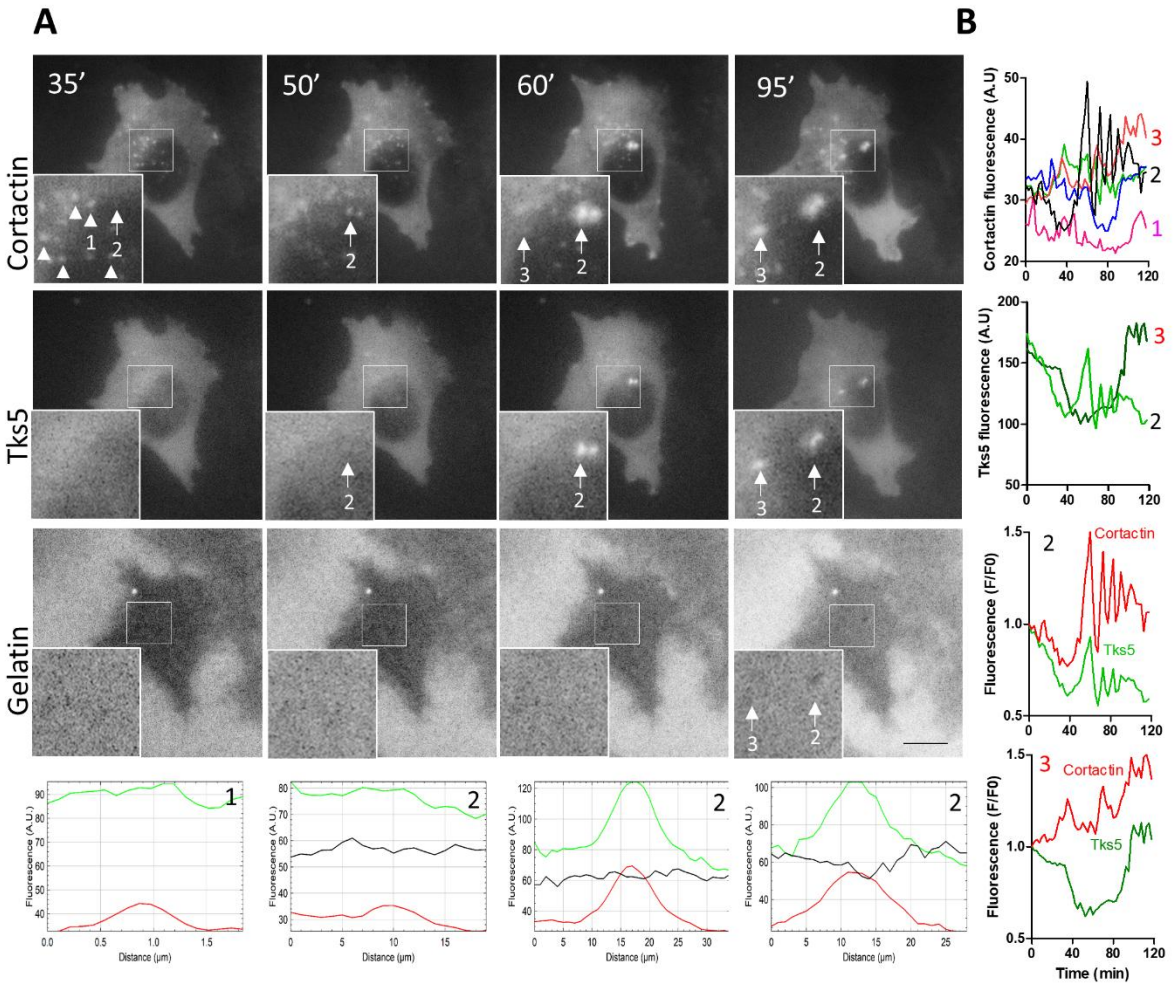
A
B
35′
50′
60′
95′
Cortactin
Tks5
Gelatin
Cortactin fluorescence (A.U)
Tks5 fluorescence (A.U)
Fluorescence (F/F0)
Cortactin
Tks5
Distance (μm)
Time (min)

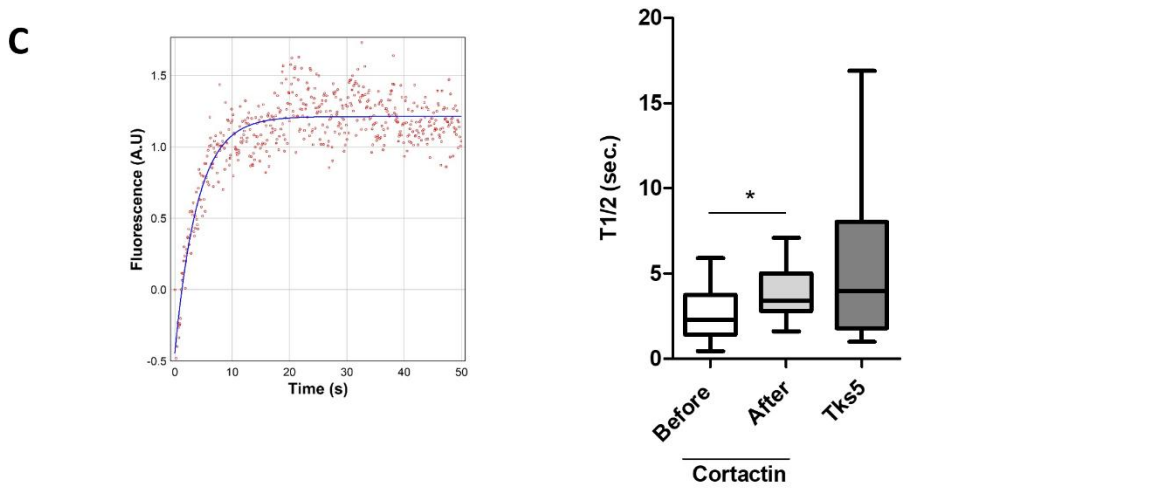
C
Fluorescence (A.U)
Time (s)
T1/2 (sec.)
Before
After
Tks5
Cortactin
*

Figure 2

599

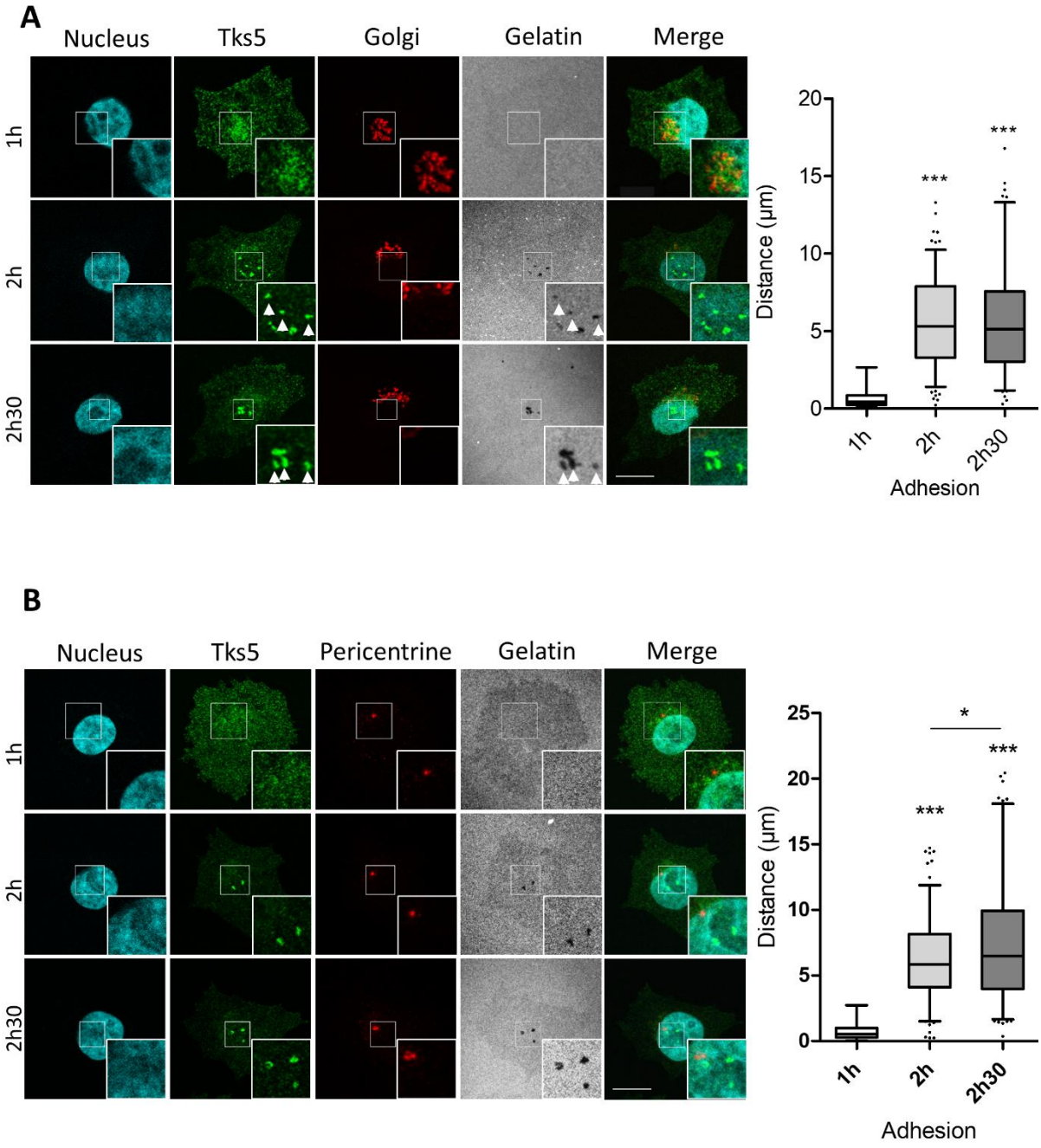
A
Nucleus
Tks5
Golgi
Gelatin
Merge
1h
2h
2h30
Distance (µm)
Adhesion
B
Nucleus
Tks5
Pericentrine
Gelatin
Merge
1h
2h
2h30
Distance (µm)
Adhesion

Figure 3

600

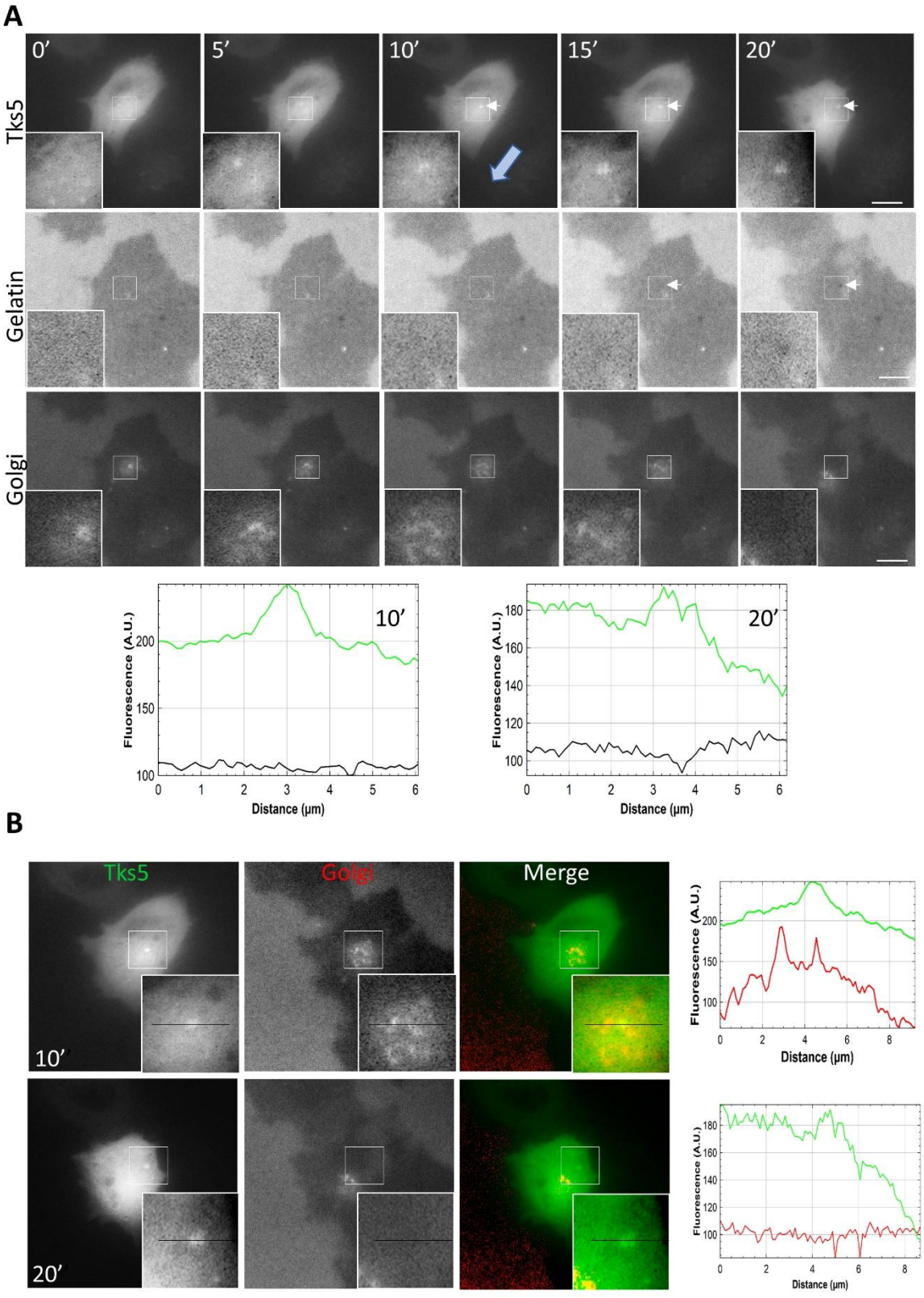
A
0′
5′
10′
15′
20′
Tks5
Gelatin
Golgi
Fluorescence (A.U.)
Distance (μm)
10′
20′
B
Tks5
Golgi
Merge
10′
20′

Figure 4

601

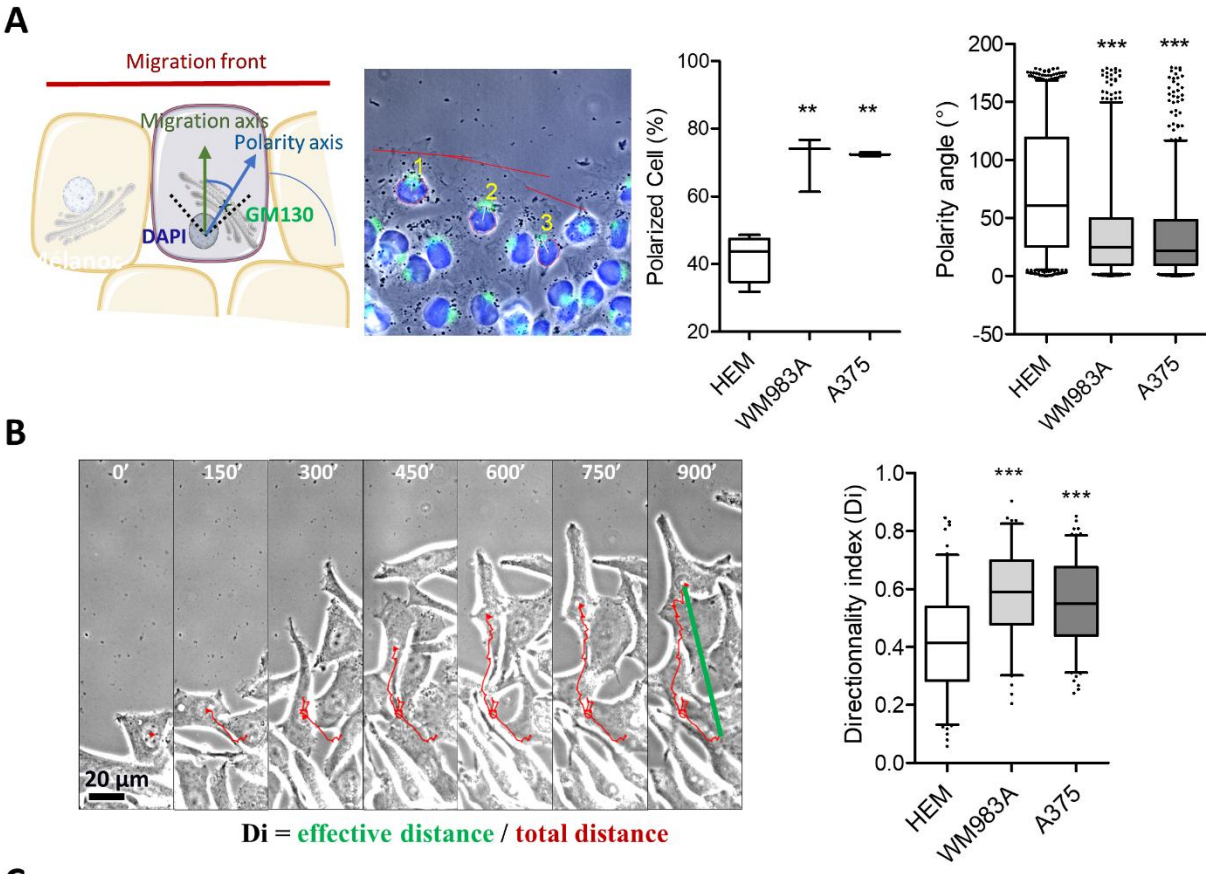
A
Migration front
Migration axis
Polarity axis
GM130
DAPI
Polarized Cell (%)
Polarity angle (°)
HEM
WM983A
A375
B
0'
150'
300'
450'
600'
750'
900'
20 µm
Directionnality index (Di)
Di = effective distance / total distance
C
Tubulin
0'
15'
25'
35'
D
Tubulin
Tks5
0'
40'
Gelatin

Figure 5

602

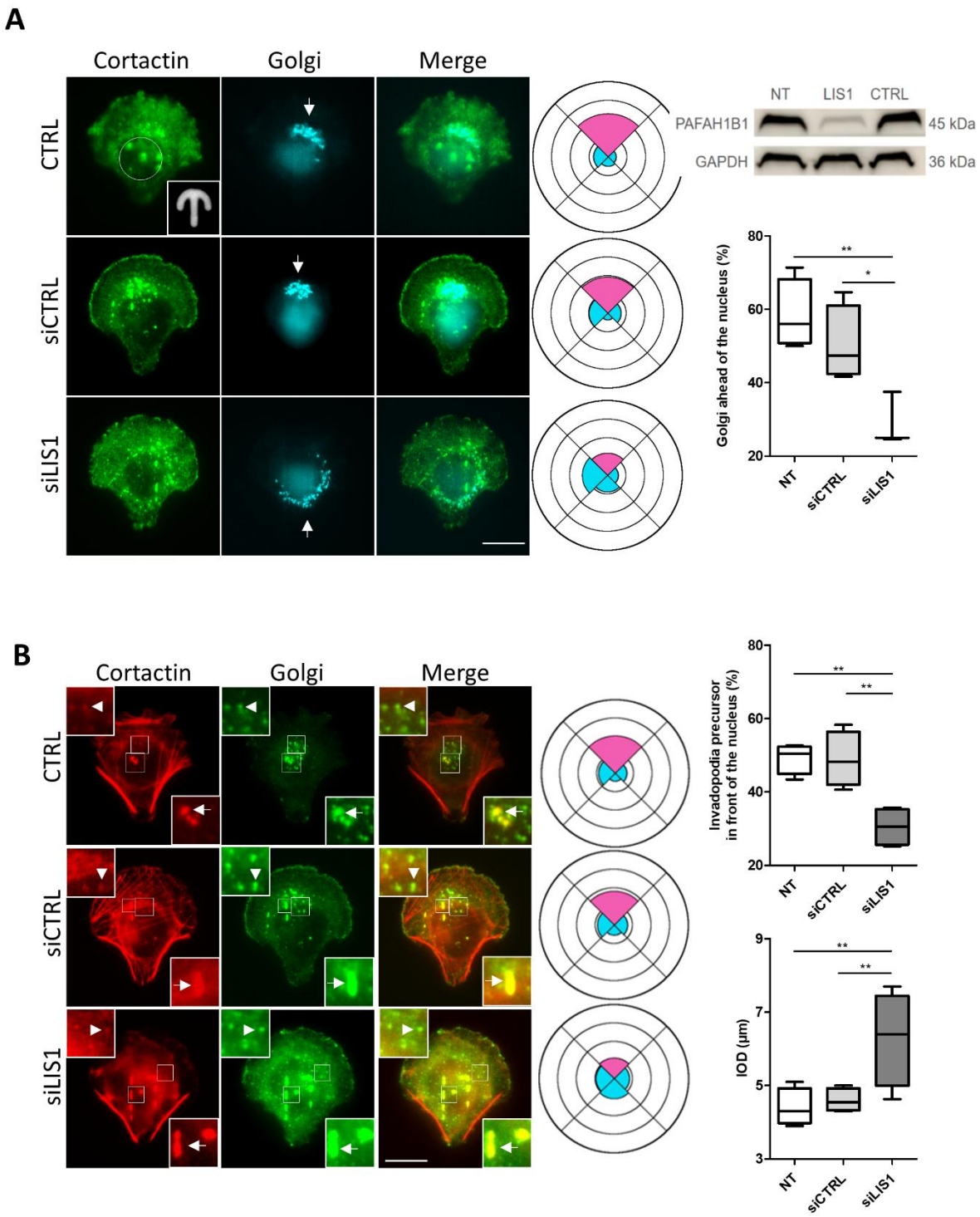
A
Cortactin
Golgi
Merge
CTRL
siCTRL
siLIS1
NT
LIS1
CTRL
PAFAH1B1
45 kDa
GAPDH
36 kDa
Golgi ahead of the nucleus (%)
80
60
40
20
**
*
NT
siCTRL
siLIS1
B
Cortactin
Golgi
Merge
CTRL
siCTRL
siLIS1
Invadopodia precursor in front of the nucleus (%)
80
60
40
20
**
**
NT
siCTRL
siLIS1
IOD (µm)
9
7
5
3
**
**
NT
siCTRL
siLIS1

Figure 6

603

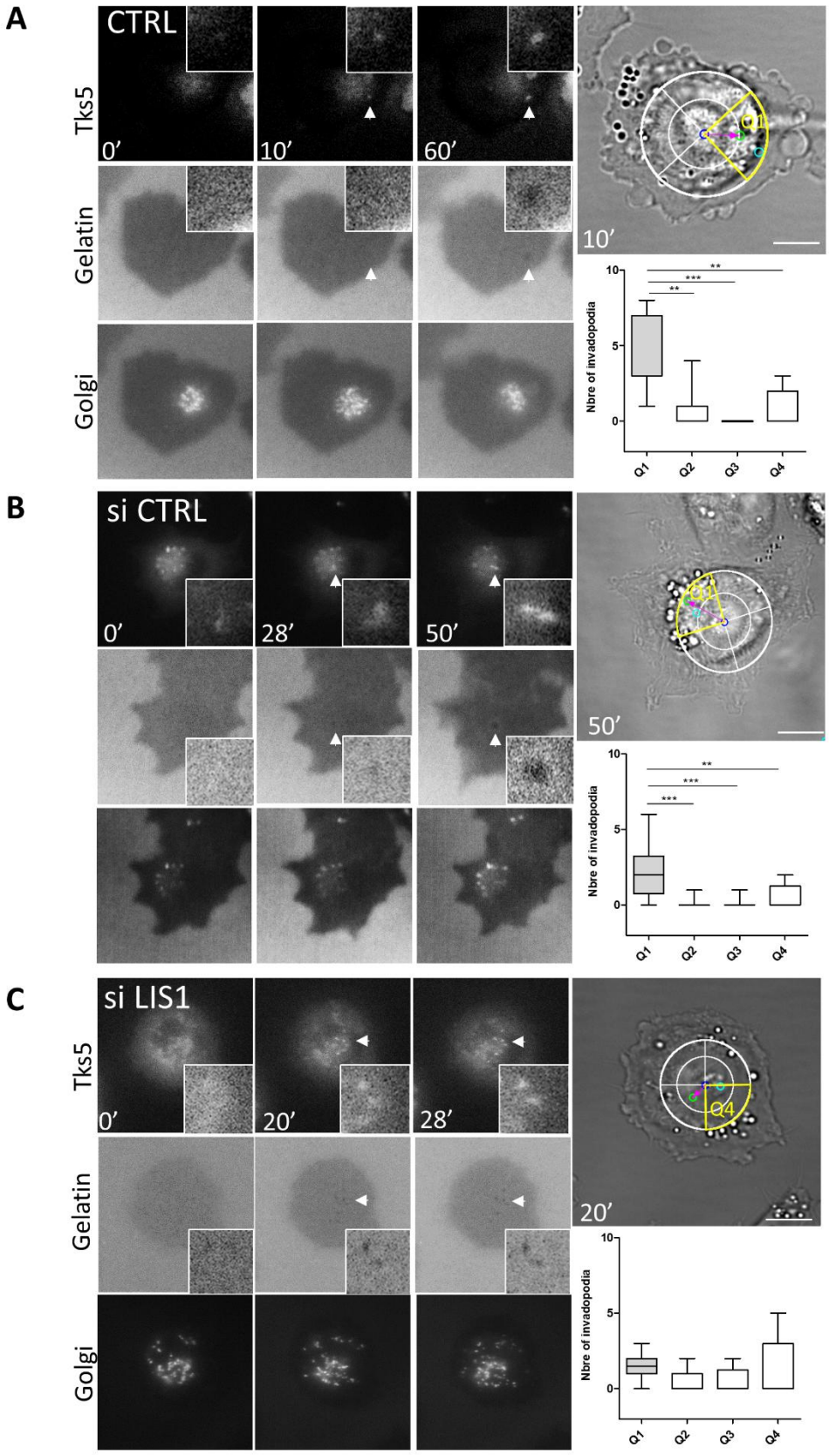
A
CTRL
Tks5
Gelatin
Golgi
0'
10'
60'
Q1
10'
Nbre of invadopodia
Q1
Q2
Q3
Q4
B
si CTRL
0'
28'
50'
Q1
50'
Nbre of invadopodia
C
si LIS1
Tks5
Gelatin
Golgi
0'
20'
28'
Q4
20'
Nbre of invadopodia

Figure 7

604

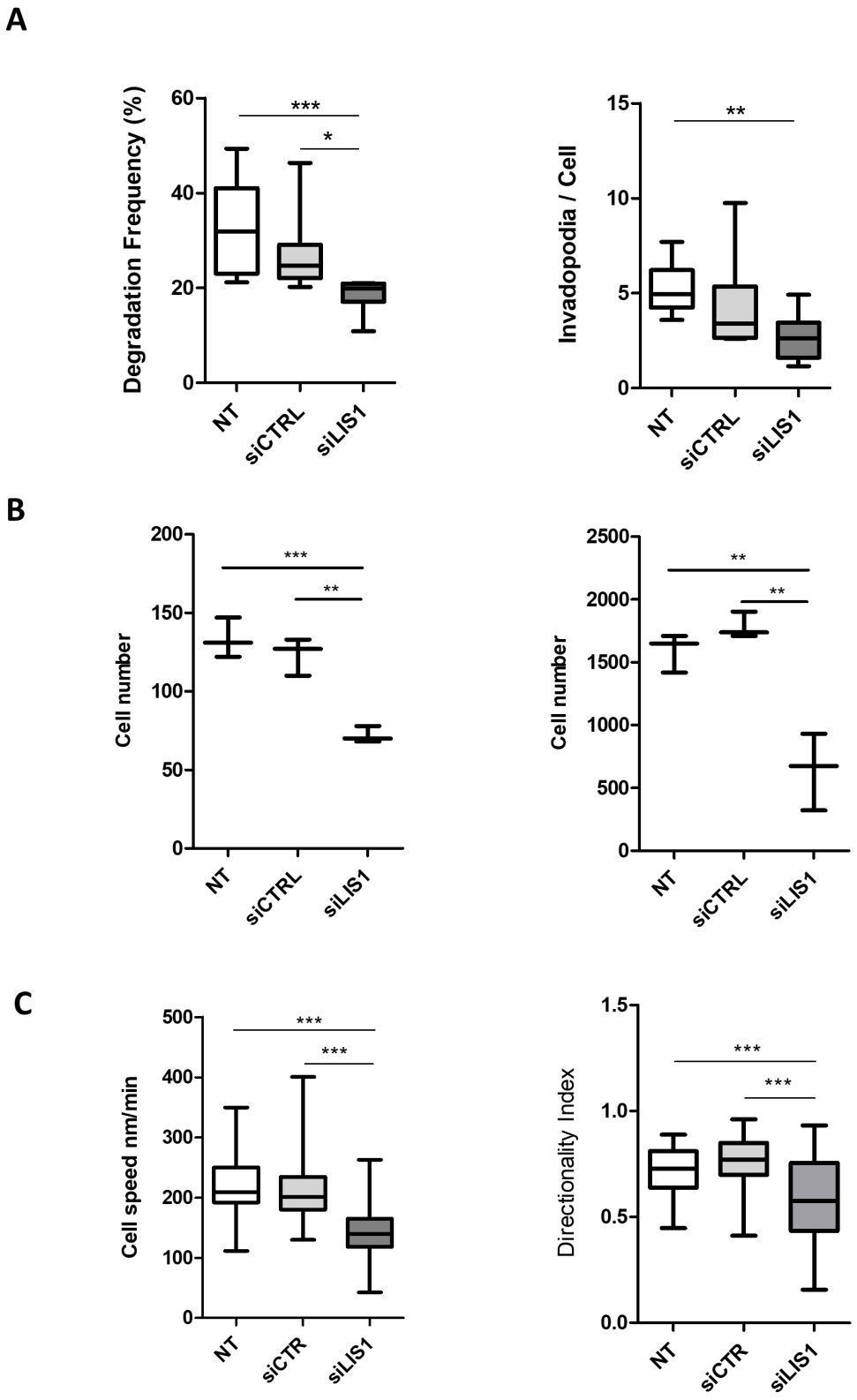

Figure 8

605

606 **ure 1: Cortactin is a marker of nascent invadopodia.** A375 melanoma cells were plated on

fluorescent gelatin (gray), fixed at different times, labelled for Tks5 (**A**, green), P-Pyk2 (**B**, green), actin (red) and cortactin (magenta) and observed using confocal microscopy. Inserts show close-up views of invadopodia. Degradation areas are identified as black regions on gelatin. Fluorescence intensity of Tks5 or P-Pyk2 (green), actin (red), cortactin (magenta) and gelatin (black) over the indicated line are portrayed on the graphs in arbitrary units (A.U.). Scale bar: 10 µm. **(C)** A375 melanoma cells were plated on gelatin, fixed at different times, stained with Dapi (cyan) and labelled for Tks5 (green), actin (red) and cortactin (magenta) and observed using confocal microscopy. Boxed regions, inserts and arrowheads show invadopodia. The box-plot indicates cortactin/actin fluorescence intensity ratios at invadopodia measured from at least 16 cells per condition from 3 independent experiments. ***P < 0.001 ; ANOVA followed by Tukey's multiple comparison test. Scale bar: 10 µm.

Figure 2: Invadopodia precursor stabilized upon Tks5 interaction with cortactin. (A) A375 melanoma cells were transfected with cortactin-dsRed and Tks5-GFP, plated on fluorescent gelatin and observed using time-lapse videomicroscopy for 5 hours at 1 image / 2.5 min (120 images in total). Representative images are shown. Inserts (white) show close-up view of cortactin structures as well as mature invadopodia in the cortactin and Tks5 channels. Arrowheads show highly dynamic cortactin-structures. Arrows depict invadopodia precursors that mature into fully degradative invadopodia upon Tks5 arrival with their respective degradation areas identified as black dots on gelatin (see for example invadopodia 2). Scale bar: 10 µm. The graphs below represent fluorescence intensity of cortactin-dsRed, Tks5-GFP and gelatin at native invadopodia (1) and invadopodia (2) during maturation for each representative image in arbitrary units (A.U.). **(B)** Graph represents the mean intensity of Cortactin-dsRed (Top) and Tks5 fluorescence (Middle top) over time of invadopodia precursor and invadopodia during maturation. Graph represents normalised fluorescence intensity over time of Cortactin-

dsRed and Tks5 fluorescence at invadopodia 2 (Middle bottom) and 3 (Bottom). **(C)** Analysis of protein dynamics at invadopodia by FRAP. Left, a typical recovery curve of Cortactin-dsRed at invadopodia is shown. Right, box chart represents the $t_{1/2}$ from 10 to 35 cells analysed per condition. Cortactin-dsRed dynamic was measured before and after invadopodia maturation. *P < 0.05 unpaired *t* test.

Figure 3: Invadopodia assemble near the centrosome. (A) A375 melanoma cells were plated on fluorescent gelatin (gray), fixed at different times, stained with Dapi (cyan), labelled for Tks5 (green) and GM130 (red, Golgi) and observed using confocal microscopy. Boxed regions, inserts and arrowheads show invadopodia and their respective degradation areas identified as black dots on gelatin. The box-plot depict invadopodia-Golgi centroids distances at different times. Distances were measured for at least 15 cells per condition from 3 independent experiments. ***P < 0.001; ANOVA followed by Tukey's multiple comparison test. Scale bar: 10 µm. **(B)** A375 melanoma cells were plated on fluorescent gelatin (gray), fixed at different times, stained with Dapi (cyan), labelled for Tks5 (green), and pericentrin (red) and observed using confocal microscopy. Boxed regions and inserts depict invadopodia and their respective degradation areas identified as black dots on gelatin. The box-plot depict invadopodia-pericentrin centroids distances at different times. Distances were measured for at least 16 cells from 3 independent experiments. ***P < 0.001 ; *P < 0.05 ; ANOVA followed by Tukey's multiple comparison test. Scale bar: 10 µm.

Figure 4: Invadopodia assemble in the vicinity of the Golgi/centrosome. (A) Live-imaging of A375 melanoma cells plated on fluorescent gelatin and expressing both Tks5-GFP and the human Golgi resident enzyme N-acetylgalactosaminyltransferase-RFP. Cells were monitored

for 5 h and images were acquired every 2.5 min for a total of 120 images. Representative images are shown every 5 min. Inserts and arrows show close-up views of invadopodia and their respective degradation areas identified as black dots on gelatin. The blue arrow indicates cell migration direction. The graphs represent fluorescence intensity of Tks5 (green) and gelatin (black) at invadopodia sites at t=10 min and t=20 min. Scale bar: 10 µm. **(B)** Tks5, Golgi and merge images at 10 min intervals are shown. Plot profiles of Tks5 (green) and Golgi (red) fluorescence intensity at invadopodia sites. Fluorescence was quantified at t=10 min and t=20 min over the indicated black scan line.

Figure 5: Melanoma are polarized cells. (A) Confluent cell layers of in-situ human melanoma cells A375 and WM983A as well as normal human melanocytes (HEM) were wounded and allowed to migrate for 3 h. The cells were then fixed, stained with Dapi (blue) and labelled for GM130 (green) as an indirect indicator of the centrosome localization. The migration axis of the cells was defined as a line starting from the centroid of the nucleus and perpendicular to the wound. The centrosome localization in relation to the migration axis was analyzed. The polarity angle was defined as a line passing through the nucleus and the Golgi centroids. A polarity angle limit of 45° was used as a cutoff value to determine whether the cells are polarized or not. The box-plot represents the percentage of polarized melanocytes and melanoma cells. Polarization was measured for 538 to 841 cells from 3 independent experiments. **$P < 0.01$; ANOVA followed by Tukey's multiple comparison test. Scale bar: 15 µm. **(B)** Confluent cell layers were wounded and cells allowed to migrate for 16 h. Cells were observed using bright field microscopy and images were acquired every 10 min. The directionality index (Di) was defined as the effective distance over the total migration distance of the cells. The red trail shows the total migration distance while the green line shows the effective distance. The box-plot represents the directionality index measured for 91 to 142 cells from 3 independent

experiments; ***P < 0.001; ANOVA followed by Tukey's multiple comparison test. Scale bar: 20 µm. **(C)** A375 melanoma cells expressing Tubulin-GFP were plated on fluorescent gelatin and observed using time-lapse videomicroscopy. Images depict polarized MTOC located ahead of the nucleus in the direction of migration. The position of the MTOC was tracked over time (graphical representation on the right). The blue arrow represents the direction of cell migration. **(D)** A375 melanoma cells expressing Tubulin-RFP and Tks5-GFP were plated on fluorescent gelatin and observed using time-lapse videomicroscopy. Tubulin and Tks5 images are shown at t=0 min and t=40 min (left). Inserts and arrowheads depict close-up views of Tks5 located along microtubules. Tks5 and gelatin images are shown (right). Note the absence of both Tks5 dot and gelatin degradation during migration. The blue arrow shows the direction of cell migration. The position of the MTOC was tracked over time (graphical representation on the right). Scale bar: 10 µm.

Figure 6: Centrosome localization regulates invadopodia precursor positioning. (A, left) A375 melanoma cells were treated with either a non-targetting pool of siRNA (siCTRL), siRNA anti-LIS1 (siLIS1) or no siRNAs at all (NT, no treatment). 48 h post-treatment, cells were plated on micropatterns and left to adhere for 4 hours. Cells were fixed and labelled for cortactin (green) and GM130 (cyan) and observed using fluorescent microscopy. Arrows depict the Golgi apparatus. Scale bar: 4 µm. **(A, Center)** The radar depictions represent the localization of the Golgi centroids in regards to the nucleus centroid. Centered on the nucleus, the cell is divided into four 90° quadants. The pink and cyan quadrants correspond to the percentage of cells with a Golgi centroid localized ahead of the nucleus or not respectively. Each circle of the radar represents a 25% limit. This polarity was measured for more than 100 cells per condition from 4 independent experiments. **(A, right)** The western blot shows the inhibition of LIS1 synthesis after each treatment. The box-plot on the right represents the percentage of cells with a Golgi

centroid ahead of the nucleus for each condition. *P < 0.05 ; **P < 0.01 ; ANOVA followed by Tukey's multiple comparison test. **(B, left)** A375 melanoma cells were treated as before, fixed, labelled for actin (red) and cortactin (green) and observed using fluorescent microscopy. The boxed regions and the inserts show close-up view of invadopodia. Arrows show mature invadopodia identified by their high cortactin and actin signals. Arrowheads show precursors of invadopodia with cortactin and actin signals of lesser intensity. Scale bar: 4 µm. The radar representations illustrate the localization of invadopodia precursors in regards to the nucleus centroid as before. This polarization was measured for more than 100 cells per conditions from 4 independent experiments. The box-plot on the top right represents the percentage of cells with invadopodia ahead of the nucleus for each condition. The bottom box-plot represents the Inter-Organelle Distance (IOD) between all invadopodia precursors for each condition. **P < 0.01; ANOVA followed by Tukey's multiple comparison test.

Figure 7: LIS1 controls polarized invadopodia formation in freely moving melanoma cells. Untreated **(A),** control siRNA **(B)** or anti-LIS1 siRNA **(C)** treated A375 melanoma cells expressing both Tks5-GFP and the human Golgi resident enzyme N-acetylgalactosaminyltransferase-RFP were plated on fluorescent gelatin and observed using time-lapse videomicroscopy for 5 hours with image acquisition every 2.5 min. Representative images are shown at **(A)** t=0 min, t=10 min and t=60 min or **(B)** t=0 min, t=28 min and t=50 min or **(C)** t=0 min, t=20 min and t=28 min. The inserts and arrows show invadopodia as well as their corresponding degradation areas identified as black dots on gelatin. Corresponding Bright field images of the cells at t=10 min, t=50 min and t=20 min are shown on the right. The green circle marks the centroid on the Golgi apparatus, the blue circle marks the centroid of the nucleus with the red arrow between the two circles defining the polarity axis. The cyan circle marks invadopodia positions. The box-plots represent the number of invadopodia in each of the

90° quadrants centered on the nucleus centroid. 30 to 43 invadopodia were analyzed from at least 3 independent experiments. Q1 quadrant is on each side (45°) of the polarity axis, Q2, Q3 and Q4 are the following clockwise 90° quadrants. The yellow quadrants correspond to the quadrant where invadopodia appear. **P < 0.01; ***P < 0.001; ****P < 0.0001; ANOVA followed by Tukey's multiple comparison test. Scale bar : 10 µm.

Figure 8: Lis1 knock-down reduce melanoma cell migration and invasion. (A) A375 melanoma cells untreated or expressing control or anti-LIS1 siRNA were plated on fluorescent gelatin and labelled for Tks5, actin and cortactin and observed using confocal microscopy. Degradation areas are identified as black regions on gelatin. Box-plot representation of the percentage of cells displaying gelatin degradation (Left) and the mean number of active invadopodia per cell (Right). (**B**) A375 melanoma cells untreated or expressing control or anti-LIS1 siRNA were seeded in Matrigel-coated Boyden chambers and allowed to invade for 24 h. Medium with 10% FBS was used as a chemotactic agent. For migration assays, cells were seeded in uncoated transwell inserts and allowed to migrate for 24 h. Migrating/invading cell nuclei were stained with DAPI. The box-plot represent the number of cells in the lower compartment of the transwell. **(C)** Untreated, control or anti-LIS1 siRNA confluent cell layers were wounded and cells allowed to migrate for 6 h. Cells were observed using bright field microscopy and images were acquired every 15 min. The box-plot represents cell migration speed (left) and cell directionality index (right) measured for 38 to 45 cells from 3 independent experiments *P < 0.05; **P < 0.01; ***P < 0.001; ANOVA followed by Tukey's or Dunn's multiple comparison test.

Supplemental Figure 1: Tks5-GFP and Cortactin-DsRed localize at invadopodia. (A) A375 melanoma cells were cultured on fluorescent gelatine (grey), transfected with DsRed-Cortactin (magenta), fixed and stained for actin (red) and cortactin (green). Scale bar: 15 µm.

(B) A375 melanoma cells were cultured on fluorescent gelatin (grey), transfected with Tks5-GFP (green), fixed and stained for actin (red) and Tks5 (cyan). Scale bar: 10 μm. The boxed regions and insets show invadopodia. The arrows indicate active invadopodia. Note the perfect colocalisation of tagged proteins revealed by GFP derivatives and endogenous proteins revealed by antibodies.

Video 1: Time-lapse imaging (3 channels, 1 set of images/2.5 min) of A375 cells expressing cortactin-dsRed and Tks5-GFP plated on Alexa647-Gelatin.

Video 2: Time-lapse imaging (3 channels, 1 set of images/2.5 min) of A375 cells expressing N-acetylgalactosaminyltransferase-RFP and Tks5-GFP plated on Alexa647-Gelatin.

Video 3: Time-lapse imaging (1 image/2.5 min) of A375 cells expressing Tubullin-RFP.

Video 4: Time-lapse imaging (1 images/2.5 min) of A375 cells expressing Tks5-GFP and plated on Alexa647-Gelatin.

Video 5: Time-lapse imaging (4 channels, 1 set of images/2.5 min) of A375 cells expressing N-acetylgalactosaminyltransferase-RFP and Tks5-GFP plated on Alexa647-Gelatin and transfected with control siRNA. The video shows the bright field images. The green circle marks the centroid on the Golgi apparatus, the blue circle marks the centroid of the nucleus

with the red arrow between the two circles defining the polarity axis. The cyan circle marks invadopodia positions. The white circle is divided into four 90° quadrants centered on the nucleus centroid. The quadrant highlighted in yellow indicate the quadrant in which invadopodia appear.

Video 6: Time-lapse imaging (4 channels, 1 set of images/2.5 min) of A375 cells expressing N-acetylgalactosaminyltransferase-RFP and Tks5-GFP plated on Alexa647-Gelatin and transfected with siLis1. The video shows the bright field images. The green circle marks the centroid on the Golgi apparatus, the blue circle marks the centroid of the nucleus with the red arrow between the two circles defining the polarity axis. The cyan circle marks invadopodia positions. The white circle is divided into four 90° quadrants centered on the nucleus centroid. The quadrant highlighted in yellow indicate the quadrant in which invadopodia appear.

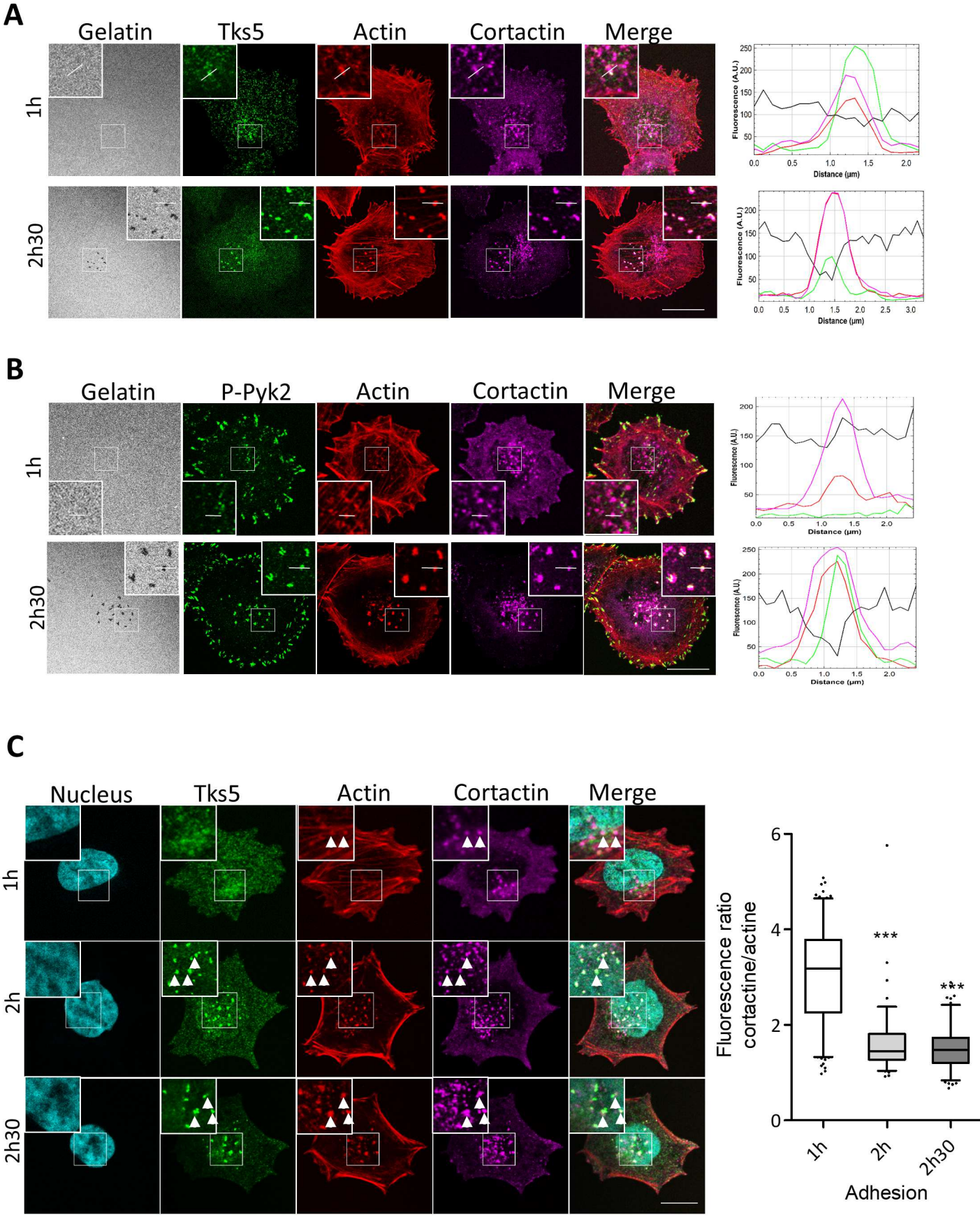
A
Gelatin
Tks5
Actin
Cortactin
Merge
1h
2h30
Fluorescence (A.U.)
Distance (µm)
B
Gelatin
P-Pyk2
Actin
Cortactin
Merge
1h
2h30
Fluorescence (A.U.)
Distance (µm)
C
Nucleus
Tks5
Actin
Cortactin
Merge
1h
2h
2h30
Fluorescence ratio cortactine/actine
***
***
1h
2h
2h30
Adhesion

Figure 1

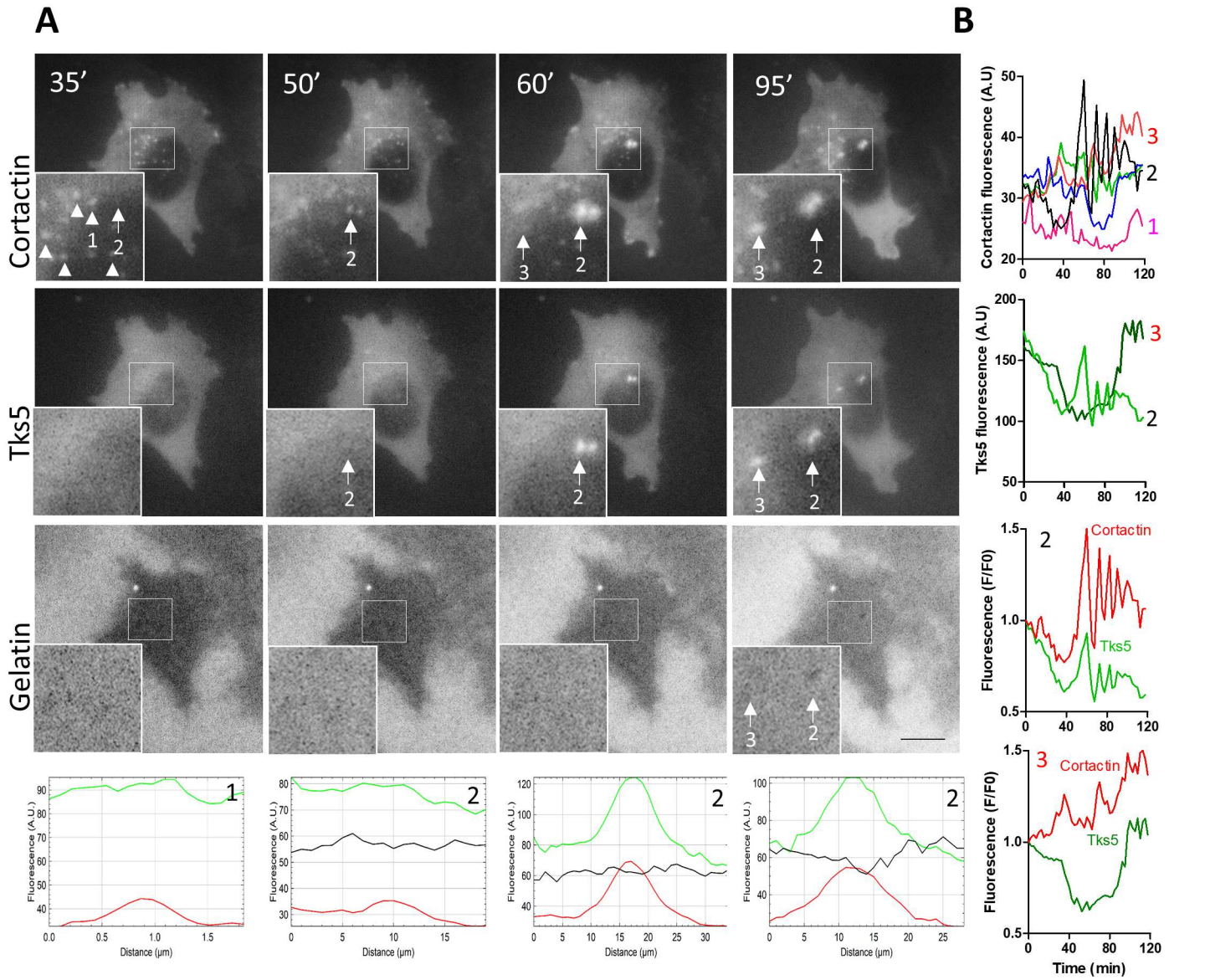
A
B
35′
50′
60′
95′
Cortactin
Tks5
Gelatin
Cortactin fluorescence (A.U)
Tks5 fluorescence (A.U)
Fluorescence (F/F0)
Cortactin
Tks5
Distance (μm)
Time (min)

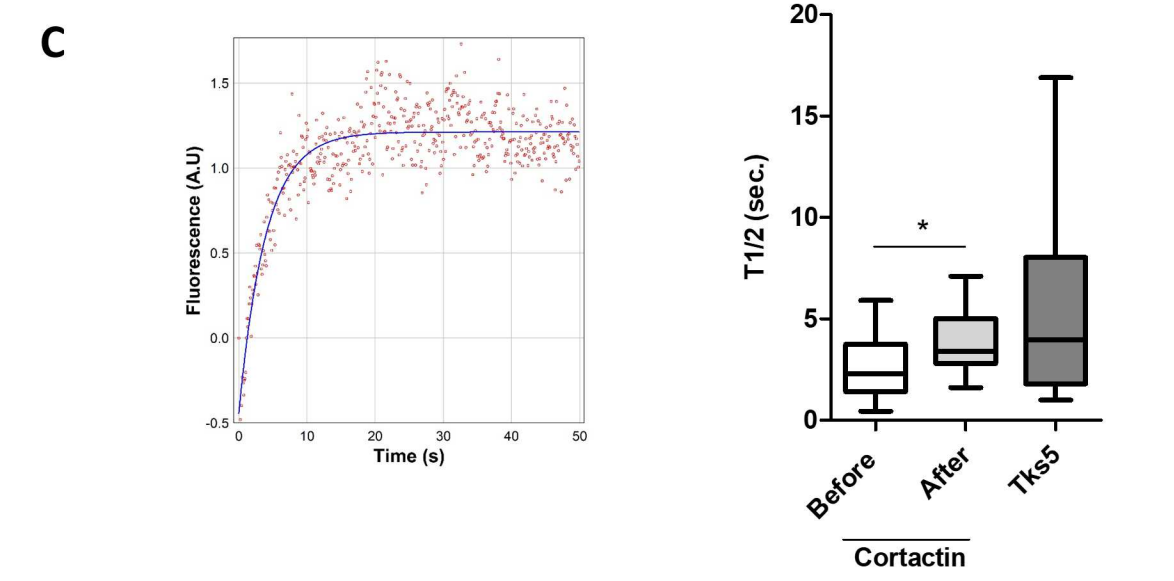
C
Fluorescence (A.U)
Time (s)
T1/2 (sec.)
Before
After
Tks5
Cortactin

Figure 2

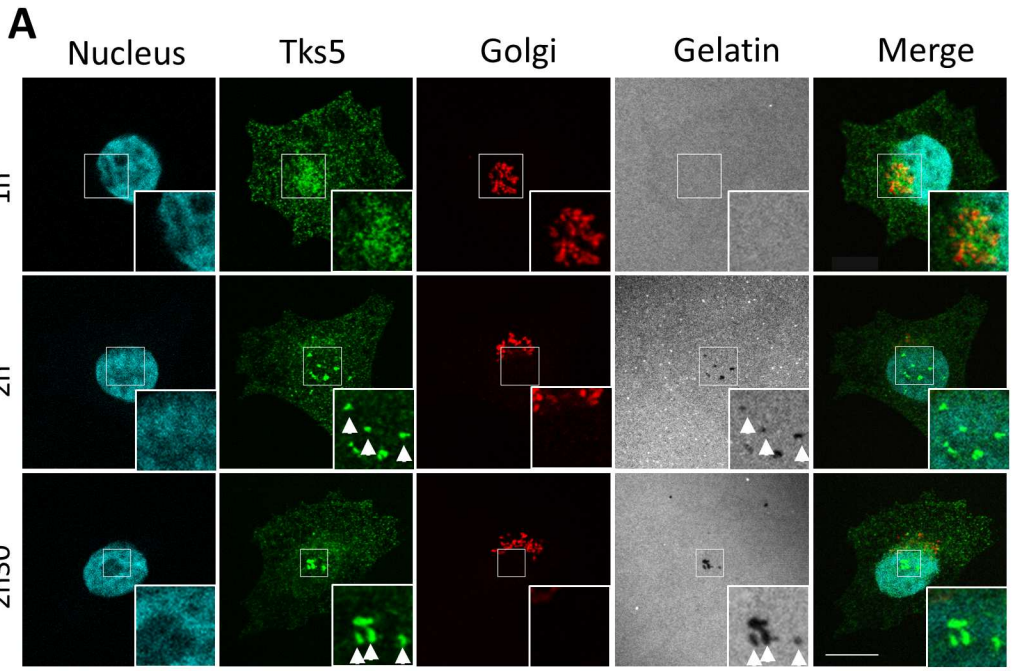
A
Nucleus
Tks5
Golgi
Gelatin
Merge
1h
2h
2h30

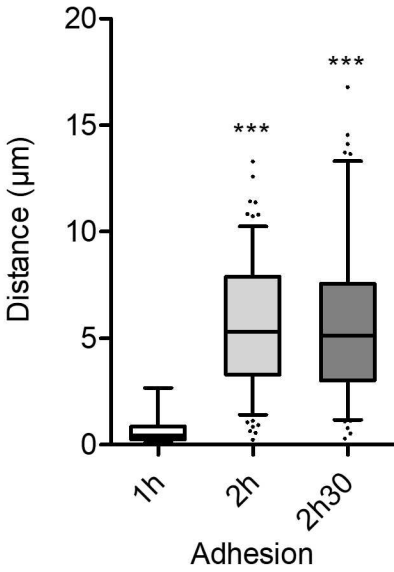
Distance (µm)
20
15
10
5
0
***
***
1h
2h
2h30
Adhesion

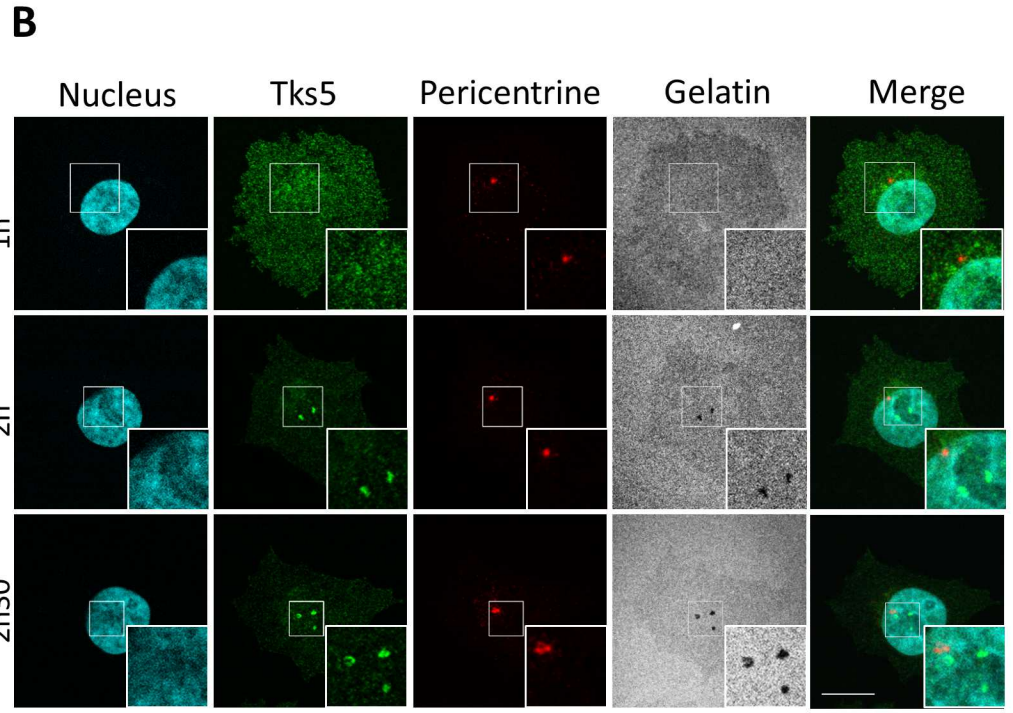
B
Nucleus
Tks5
Pericentrine
Gelatin
Merge
1h
2h
2h30

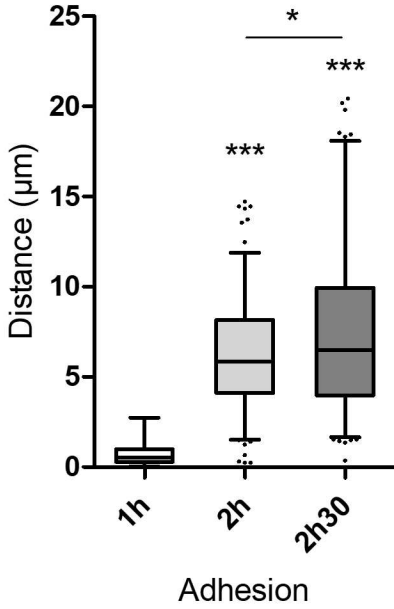
Distance (µm)
25
20
15
10
5
0
*
***
***
1h
2h
2h30
Adhesion

Figure 3

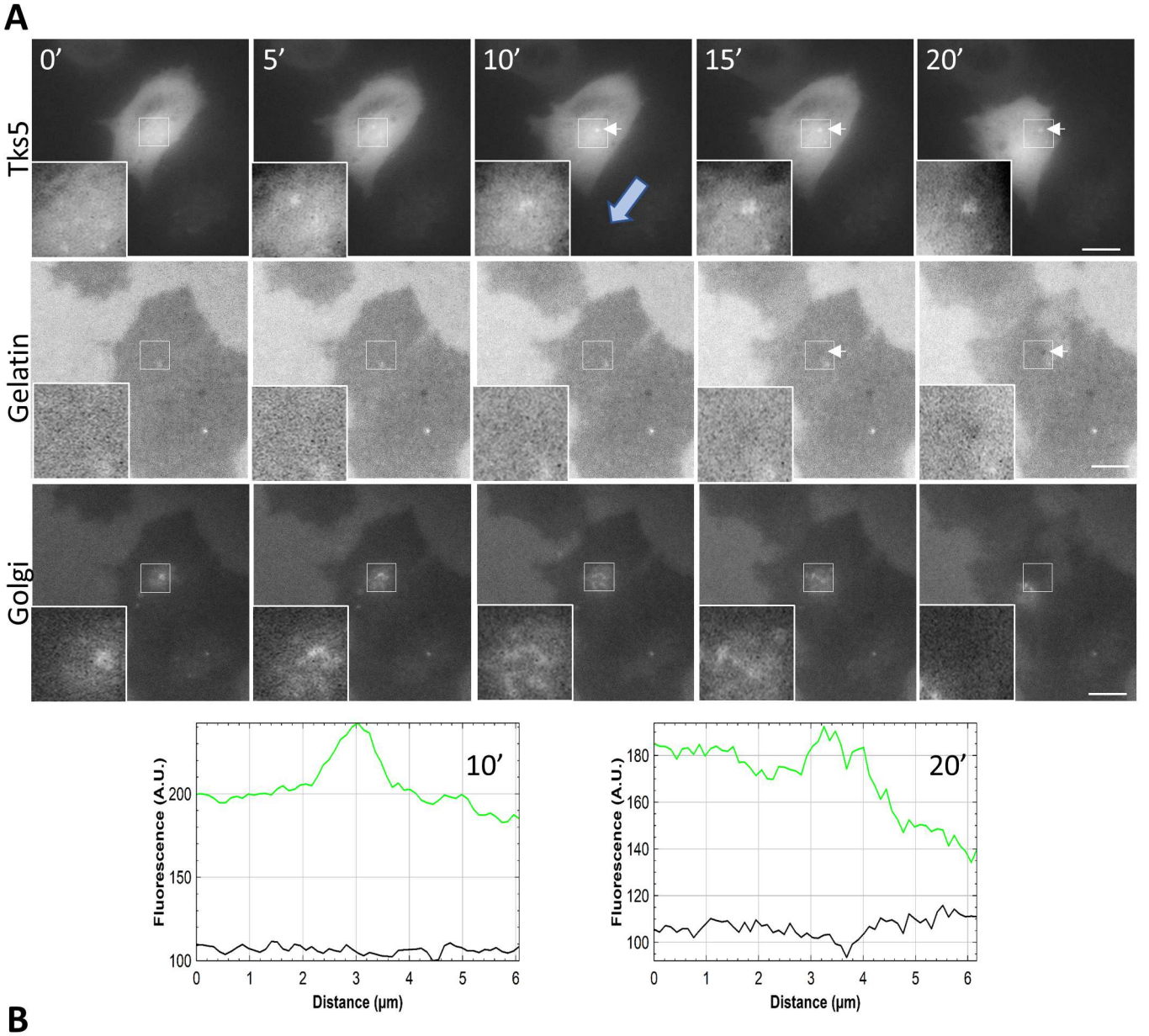
A
0′
5′
10′
15′
20′
Tks5
Gelatin
Golgi
10′
20′
Fluorescence (A.U.)
Distance (μm)

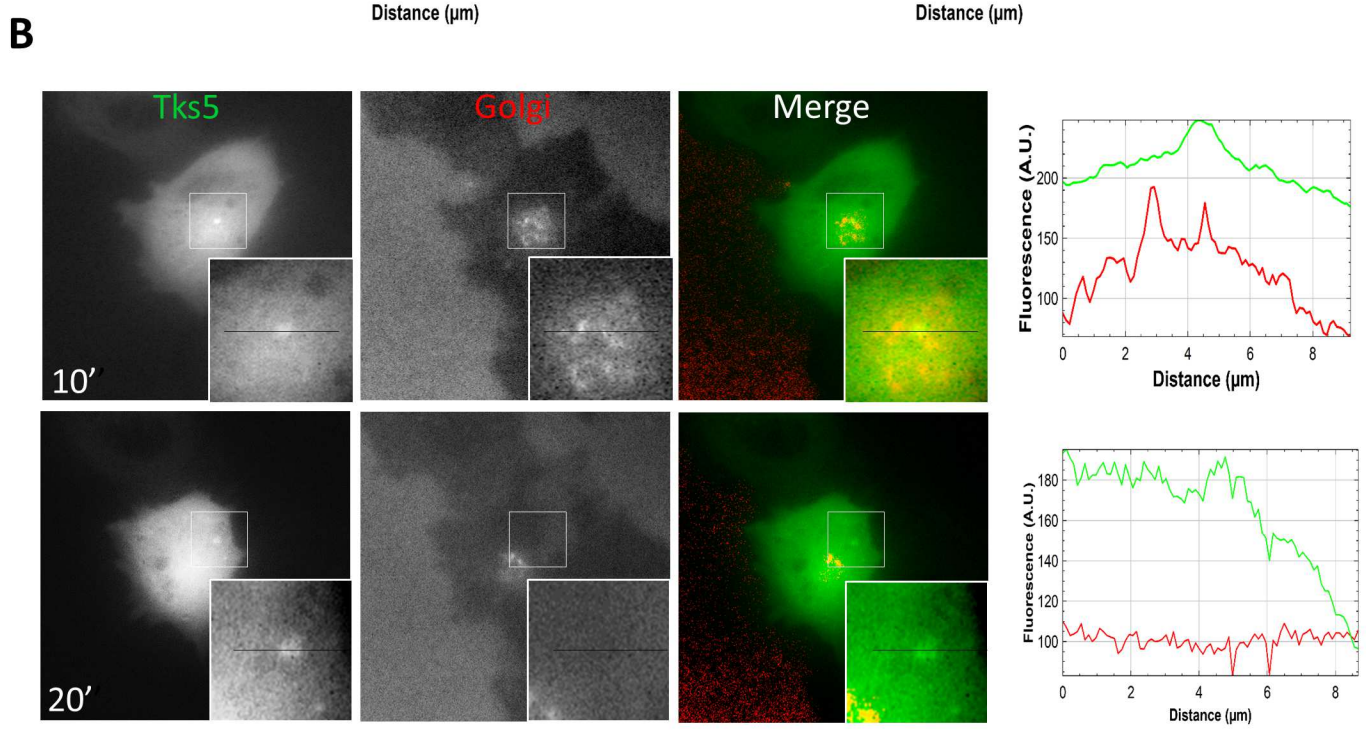
B
Tks5
Golgi
Merge
10′
20′
Fluorescence (A.U.)
Distance (μm)

Figure 4

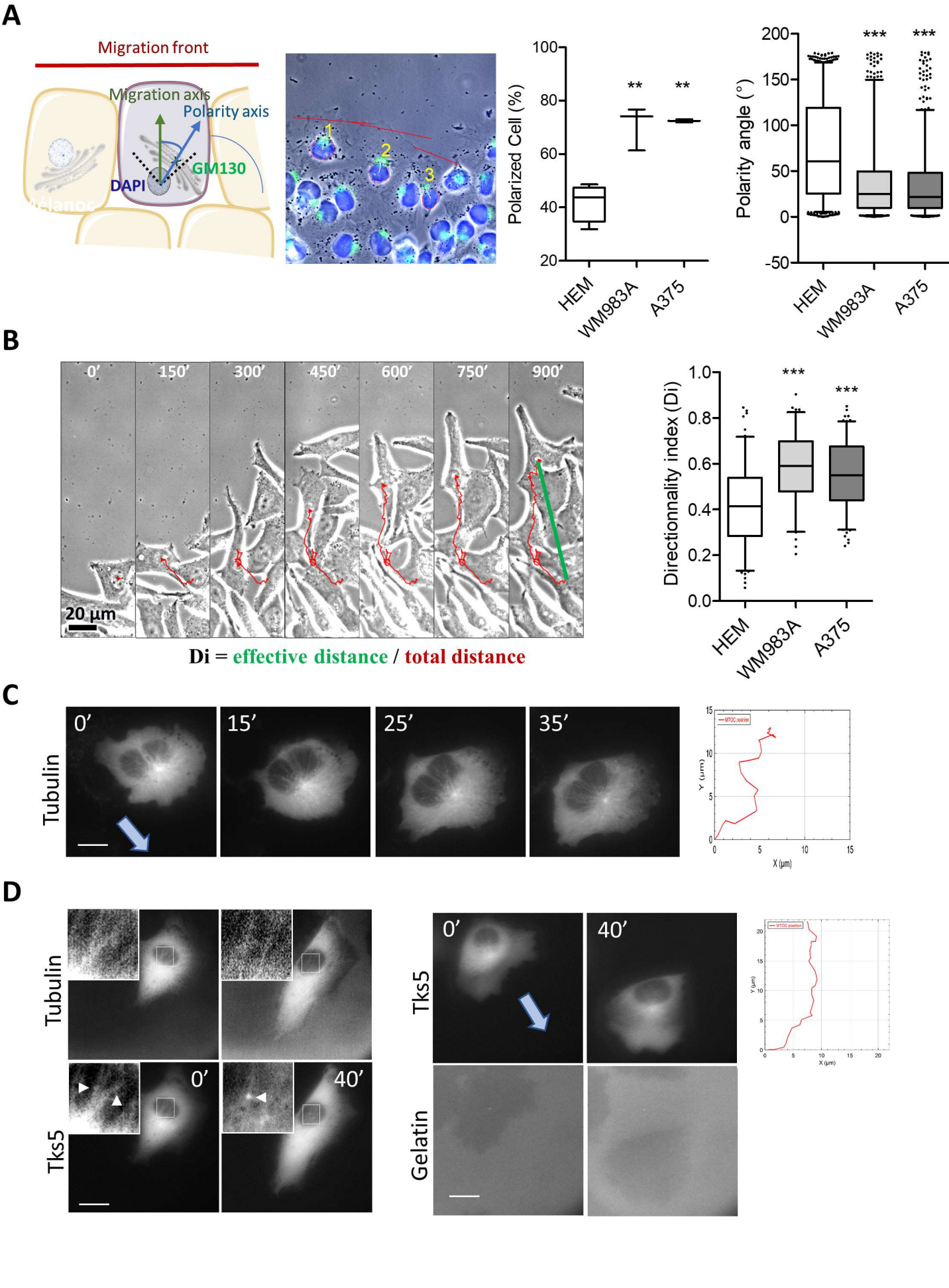
A
Migration front
Migration axis
Polarity axis
GM130
DAPI
1
2
3
Polarized Cell (%)
100
80
60
40
20
**
**
HEM
WM983A
A375
Polarity angle (°)
200
150
100
50
0
-50
***
***
HEM
WM983A
A375
B
0'
150'
300'
450'
600'
750'
900'
20 µm
Di = effective distance / total distance
Directionnality index (Di)
1.0
0.8
0.6
0.4
0.2
0.0
***
***
HEM
WM983A
A375
C
Tubulin
0'
15'
25'
35'
MTOC position
Y (µm)
X (µm)
D
Tubulin
Tks5
0'
40'
Tks5
Gelatin
0'
40'
MTOC position
Y (µm)
X (µm)

Figure 5

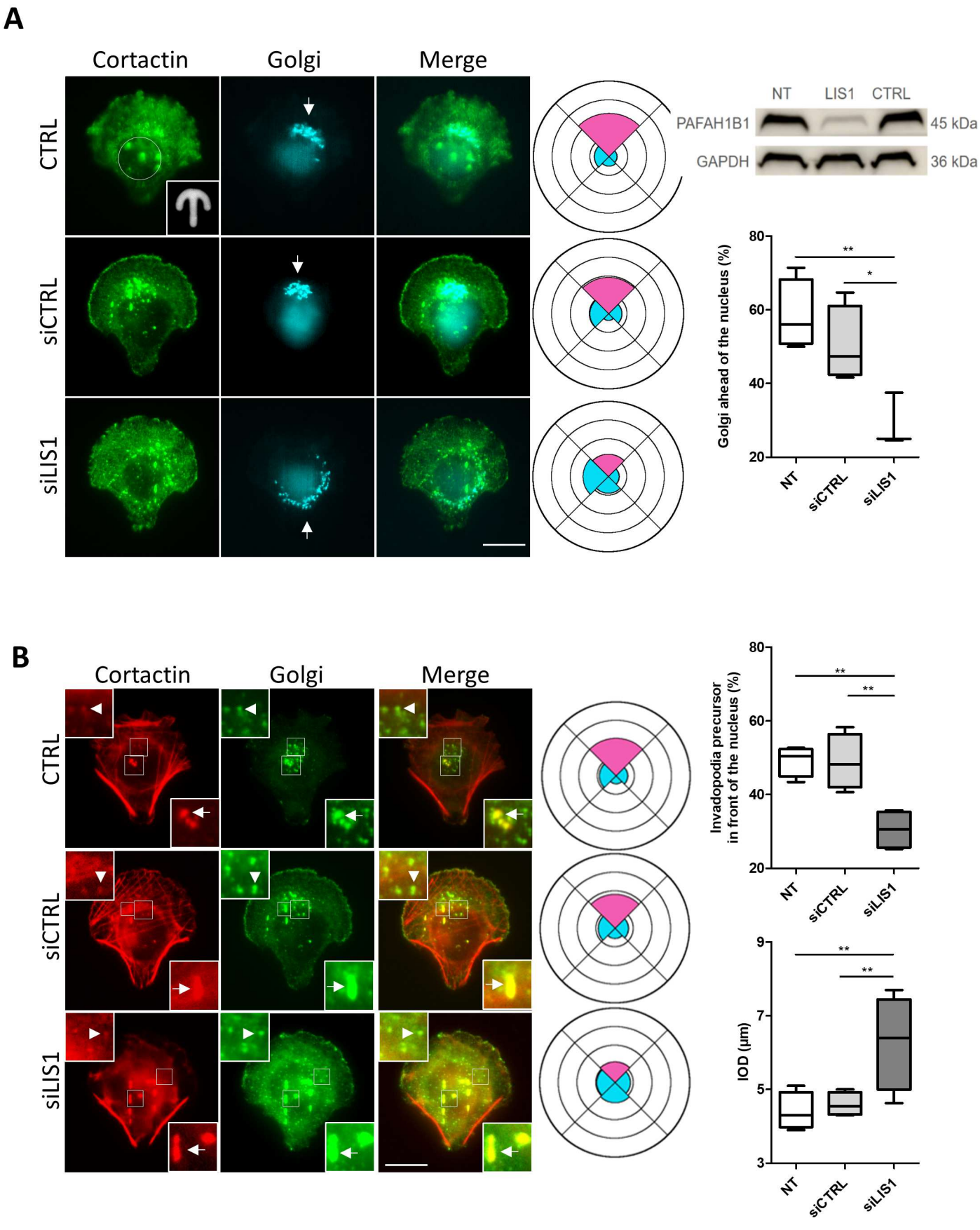
A
Cortactin
Golgi
Merge
CTRL
siCTRL
siLIS1
NT
LIS1
CTRL
PAFAH1B1
45 kDa
GAPDH
36 kDa
Golgi ahead of the nucleus (%)
80
60
40
20
**
*
NT
siCTRL
siLIS1
B
Cortactin
Golgi
Merge
CTRL
siCTRL
siLIS1
Invadopodia precursor in front of the nucleus (%)
80
60
40
20
**
**
NT
siCTRL
siLIS1
IOD (µm)
9
7
5
3
**
**
NT
siCTRL
siLIS1

Figure 6

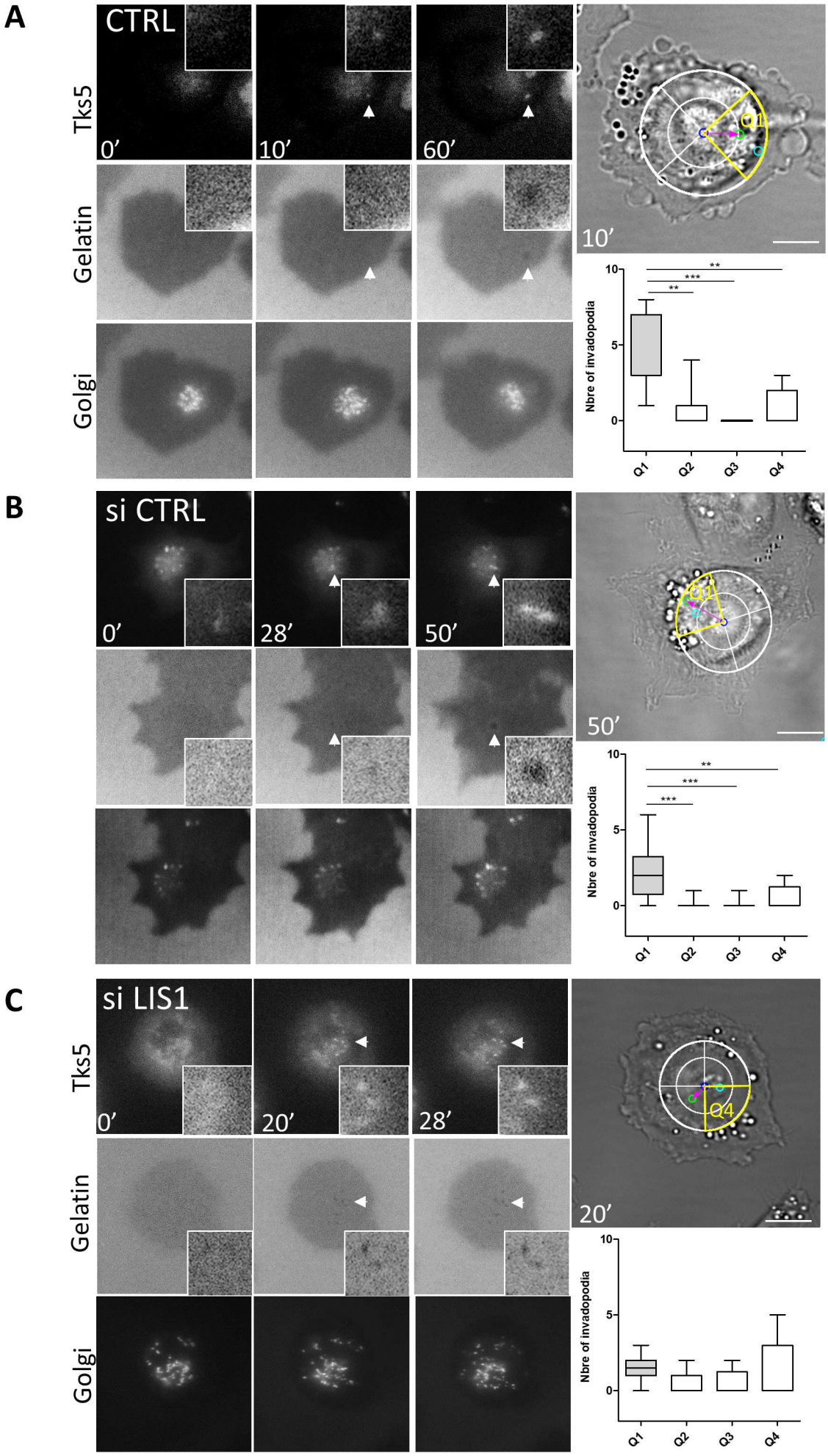
A
CTRL
Tks5
Gelatin
Golgi
0'
10'
60'
Q1
10'
Nbre of invadopodia
Q1
Q2
Q3
Q4
B
si CTRL
0'
28'
50'
Q1
50'
Nbre of invadopodia
C
si LIS1
Tks5
Gelatin
Golgi
0'
20'
28'
Q4
20'
Nbre of invadopodia

Figure 7

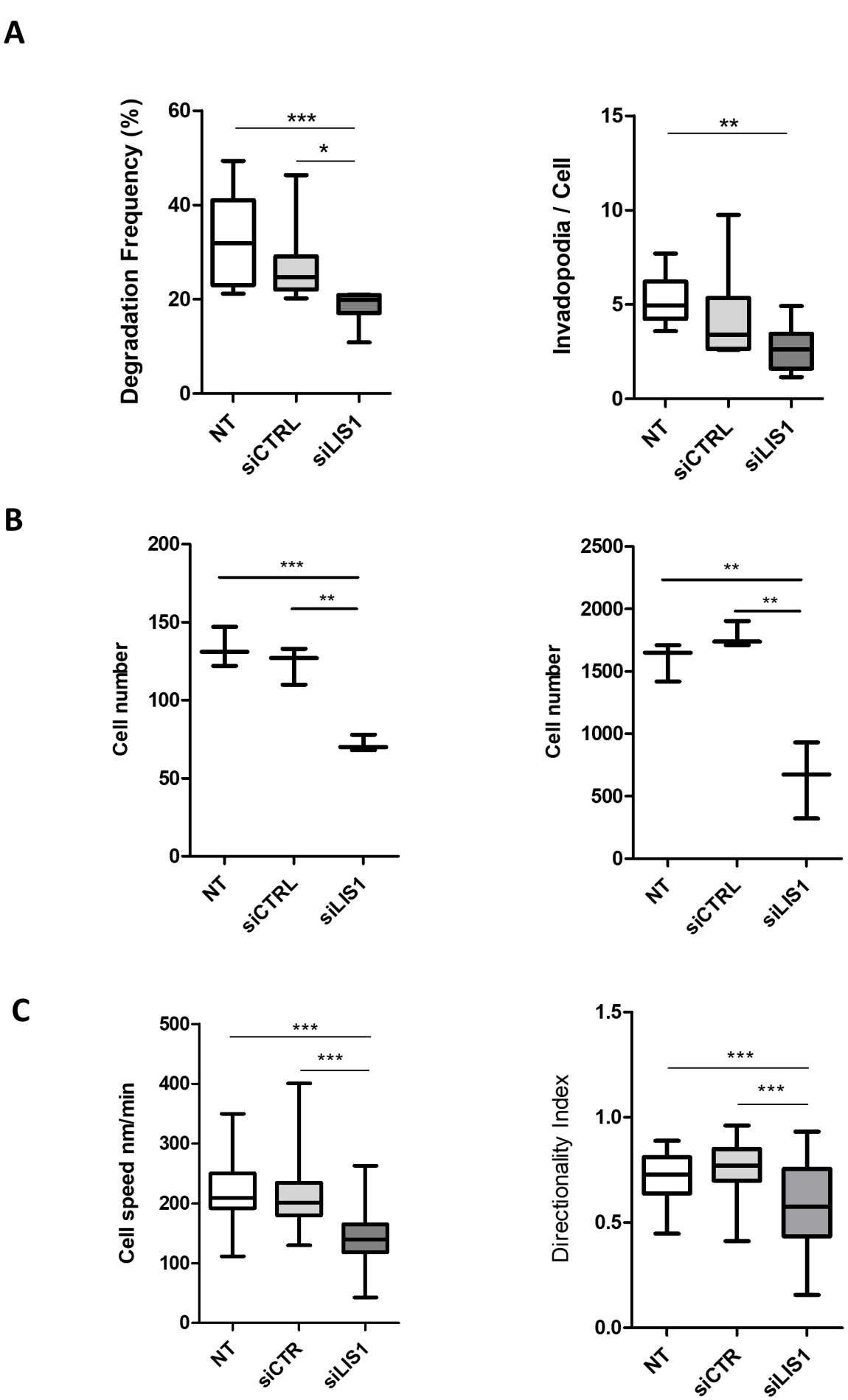
A
Degradation Frequency (%)
60
40
20
0
***
*
NT
siCTRL
siLIS1
Invadopodia / Cell
15
10
5
0
**
NT
siCTRL
siLIS1
B
Cell number
200
150
100
50
0
***
**
NT
siCTRL
siLIS1
Cell number
2500
2000
1500
1000
500
0
**
**
NT
siCTRL
siLIS1
C
Cell speed nm/min
500
400
300
200
100
0
***
***
NT
siCTR
siLIS1
Directionality Index
1.5
1.0
0.5
0.0
***
***
NT
siCTR
siLIS1

Figure 8

Supplementary Files

This is a list of supplementary files associated with this preprint. Click to download.

- Video3.avi
- Video4.avi
- Video5.avi
- Video2.avi
- Video1.avi
- SupplementalFigure1.tif
- Video6.avi